Hindawi
Shock and Vibration
Volume 2017, Article ID 8186976, 23 pages
https://doi.org/10.1155/2017/8186976

Research Article

A Normalized Transfer Matrix Method for the Free Vibration of Stepped Beams: Comparison with Experimental and FE(3D) Methods

Tamer Ahmed El-Sayed and Said Hamed Farghaly

Department of Mechanical Design, Faculty of Engineering, Mataria, Helwan University, P.O. Box 11718, Helmeiat-Elzaton, Cairo, Egypt

Correspondence should be addressed to Tamer Ahmed El-Sayed; tamer_alsayed@m-eng.helwan.edu.eg

Received 2 June 2017; Revised 22 August 2017; Accepted 15 October 2017; Published 28 November 2017

Academic Editor: Toshiaki Natsuki

The exact solution for multistepped Timoshenko beam is derived using a set of fundamental solutions. This set of solutions is derived to normalize the solution at the origin of the coordinates. The start, end, and intermediate boundary conditions involve concentrated masses and linear and rotational elastic supports. The beam start, end, and intermediate equations are assembled using the present normalized transfer matrix (NTM). The advantage of this method is that it is quicker than the standard method because the size of the complete system coefficient matrix is 4×4. In addition, during the assembly of this matrix, there are no inverse matrix steps required. The validity of this method is tested by comparing the results of the current method with the literature. Then the validity of the exact stepped analysis is checked using experimental and FE(3D) methods. The experimental results for stepped beams with single step and two steps, for sixteen different test samples, are in excellent agreement with those of the three-dimensional finite element FE(3D). The comparison between the NTM method and the finite element method results shows that the modal percentage deviation is increased when a beam step location coincides with a peak point in the mode shape. Meanwhile, the deviation decreases when a beam step location coincides with a straight portion in the mode shape.

1. Introduction

Stepped beam-like structure plays an important role in the construction of mechanical and civil engineering systems. Flexural vibrations were first investigated by Euler-Bernoulli in the eighteenth century. The rotary inertia effect was considered by Rayleigh [1]. Almost 95 years ago, Timoshenko introduced a correction for the beam theory to include the shear deformation effect [2]. The effect of rotary inertia and shear deformations on the beam natural frequencies is small at the lower normal modes and large at the higher normal modes. Cowper [3] derived formulae for the precise evaluation of the shear coefficient for rectangular and round cross sections as a function of Poisson's ratio ν.

The free vibrations of beams with discontinuities can be solved using either exact or approximate solution. The exact methods include the derivation of the transcendental eigenvalue equations in order to evaluate the beam natural frequencies. In the case of relatively simple problems closed form solutions for the eigenvalue problem were obtained [4, 5].

For complicated problems, the beam eigenvalues are obtained by the decomposition of the domain. Numerical assembly technique (NAT) is one of the common methods used for the evaluation of the eigenvalue problem for beams with multiple discontinuity [6–8]. In this method, the size of the frequency equation determinant is $4n \times 4n$ for beam with n segments. Dynamic stiffness matrix is one of methods that is similar to the finite element method in assembling of the elements but with exact element rather than approximate element [9, 10]. The frequency equation determinant size for n segments is $(2n + 2) \times (2n + 2)$. The Laplace transformation method is used to obtain a solution for a Timoshenko beam mounted on elastic foundation with several combinations of discrete in-span attachments and with several combinations of attachments at the boundaries [11].

The attachments include translation and rotational springs, masses, and undamped single degree of freedom system. The characteristics equation for beam with n segments is $2n \times 2n$. The transfer matrix method (TMM) is one of the favorable methods in the analysis of multispan beams. Many researchers used it to derive the frequency equation of a complicated beam system [12–14]. The advantage of this method is that, for n segments beam, the size of the frequency equation determinant is 4×4 which reduces the computational time. On the other hand, during the formulation of the beam frequency equation $n - 1$ inverse matrix steps are required to form the final system transcendental eigenvalue problem. The use of linearly independent fundamental set of solution in solving the buckling and free vibrations of nonuniform rods was introduced by Li [15] and Li et al. [16]. This method enables obtaining the closed form solution of a multispan beam. A set of fundamental solutions which suit the analysis of single-span Timoshenko beams was introduced [17].

On the other hand, there are numerous approximate methods to approximate the eigenvalue problem for the transverse vibrations of beams [21–23]. Finite element method is one of the most dominant methods for solving the free vibration of beams. The effect of step ratios and eccentricity on the free vibration of arbitrarily beam was investigated by Ju et al. [21]. The lowest three natural frequencies of a multistep up and down cantilever beam using a global Rayleigh-Ritz formulation, component modal analyses (CMA), ANSYS®, and experimental are evaluated [24]. Adomian decomposition method (ADM) was used to obtain the effect of step ratio and step location on the beam natural frequencies [25, 26]. The free and forced vibrations of beams with either single- or multiple-step changes using the composite element method (CEM) were introduced by Lu et al. [27]. The accuracy and convergence of CEM were compared with existing theoretical and experimental results. Differential transformation method (DTM) was applied in order to analyze the natural frequencies for different geometrically and material parameters stepped Bernoulli-Euler beam [28]. The differential quadrature element method (DQEM) was proposed to analyze the free vibration problem of beams with any discontinuities in cross-section [20]. Discrete singular convolution (DSC) was proposed for solving the free vibration analysis of stepped beams [29]. The solution for multistep Timoshenko beam using both numerical assembly technique and differential transformation method is proposed by Yesilce [19]. Experimental measurements were considered as a good tool for the validation of the analytical results.

The exact free vibration of two-span Timoshenko stepped beams has been investigated by Gutierrez et al. [18] and Rossi et al. [32]. Farghaly [33] derived the exact solution for four-span Timoshenko beam with attachments. Yesilce [19] investigated the free vibration of stepped beams using exact numerical assembly technique (NAT) and using approximate differential transformation method. Recently, Farghaly and El-Sayed [6] drive the exact solution for the lateral vibration of Timoshenko beam with generalized start, end, and intermediate conditions using numerical assembly technique (NAT).

The exact free vibration of a mechanical system composed of two elastic Timoshenko segments carried on an intermediate eccentric rigid body or on elastic supports was introduced by Farghaly and El-Sayed [34]. Their analysis was based on both analytical and experimental methods. They claimed a good agreement between the analytical and experimental results. Experimental setup using electromagnetic-acoustic transducer (EMAT) was introduced by Díaz-De-Anda et al. [35]. They compared the experimental results with those obtained theoretically using Timoshenko beam theory (TBT) with one and two shear coefficients. The flexural frequencies and amplitudes for cylindrical and rectangular Timoshenko beams were examined experimentally [35]. They found that the experimental results coincide very well with theoretical predictions. The transverse vibration of Bernoulli-Euler beams with discontinuous geometry and elastic support was investigated experimentally and analytically [36].

During the last decades, many literatures were focused on the problem of free and forced vibration analysis of Timoshenko beam and the accuracy of the natural frequency predictions. To the authors' knowledge, there is not enough research that has tackled the experimental modal frequencies of stepped thick beams, computationally and experimentally. Therefore, the main aim of this work is to investigate the results of the modal frequencies for such beams using analytical, experimental, and the three-dimensional finite element FE(3D). An analytical analysis is proposed which is based on the derivation of a set of fundamental solutions that suits the analysis of Timoshenko beams. This set of solutions is used to modify the TMM to include no inverse matrix procedure which may be called normalized transfer matrix method (NTM). The comparison between the experimental NTM and FE(3D) is done for selected single-step and two-step application models. The percentage deviations between NTM and FE(3D) are investigated. The results show that the finite element results are very close to the experimental results. The study includes the effect of increasing the step ratio ($\overline{d}$), step location parameter (μ), and the length ratio. Finally, the capability of the present analysis to solve the free vibration of tapered beams has been investigated.

2. Mathematical Model

The mathematical model for beam with multiple-stepped sections is shown in Figure 1. The total length of the beam is L. The beam model is divided into n segments. The beam has $(n + 1)$ stations as shown in Figure 1. The station numbering corresponding to the start, intermediate, and end location is represented by $(1, i + 1, n + 1)$, respectively. At each station, there are linear and rotational elastic supports and concentrated mass with mass moment of inertia. As shown in Figure 1, the beam segments are described by their material and cross-sectional properties ρ_i, E_i, G_i, A_i and I_i $(i = 1, 2, \ldots, n)$, which are the density, Young's modulus of elasticity, rigidity modulus, cross-sectional area, and second moment of inertia, respectively. In this section, the frequency equation of the model is driven using the proposed normalized transfer matrix method. Since the current analysis is based on Timoshenko beam theory, the rotary inertia and

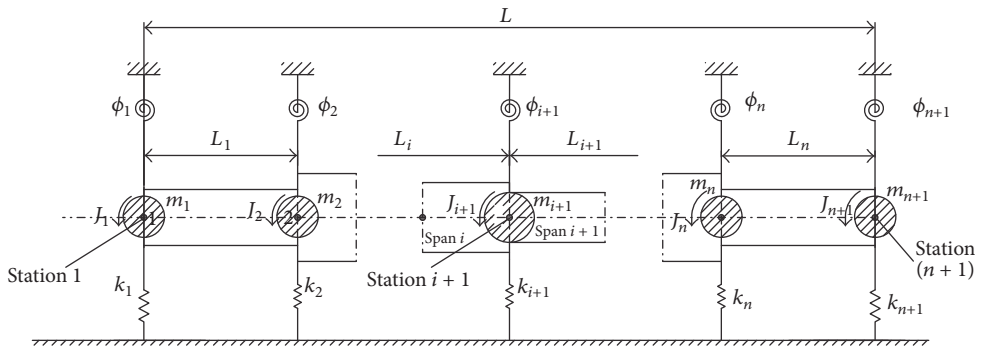

Figure 1: Stepped multispan model.

shear deformations effects are considered. In the current analysis, the analytical solution is subject to the assumptions that the shear strain is assumed constant over the cross-section; therefore, a shear coefficient k_i' is used to compensate this assumption. In addition, the effect of stress concentration at the beam steps is neglected.

2.1. Analytical Method and Frequency Equation. The objective of this section is to derive the system frequency equation which represents the model shown in Figure 1. Timoshenko differential coupled equations of motion may be written here for ith span as follows:

$$\begin{aligned}&\left(k'GA\right)_i\left(y_i'' - \psi_i'\right)(x_i,t) - \rho_i A_i \ddot{y}_i(x_i,t) = 0,\\&(EI)_i\,\psi_i''(x_i,t) - \rho_i I_i \ddot{\psi}_i(x_i,t)\\&\quad + \left(k'GA\right)_i\left(y_i' - \psi_i\right)(x_i,t) = 0.\end{aligned} \tag{1}$$

Let

$$\begin{aligned}y_i &= Y_i(\xi_i)\,e^{j\omega t},\\ \psi_i &= \Psi_i(\xi_i)\,e^{j\omega t},\\ \xi_i &= \frac{x_i}{L_i},\end{aligned} \tag{2}$$

where Y_i is the normal function of y_i, Ψ_i is the normal function of ψ_i, ξ_i is nondimensional length of each beam span i, and $j = \sqrt{-1}$.

Substituting (2) into (1) and omitting the factor $e^{j\omega t}$, the following equations can be derived:

$$Y_i''(\xi_i) + \lambda_i^4 s_i^2 Y_i(\xi_i) - L_i\Psi_i'(\xi_i) = 0, \tag{3}$$

$$s_i^2 L_i \Psi_i''(\xi_i) + \left(\lambda_i^4 r_i^2 s_i^2 - 1\right) L_i \Psi_i(\xi_i) + Y_i'(\xi_i) = 0, \tag{4}$$

where

$$\lambda_i^4 = \frac{\rho_i A_i L_i^4 \omega^2}{E_i I_i}, \tag{5a}$$

$$s_i^2 = \frac{2r_i^2(1+\nu_i)}{k_i'}, \tag{5b}$$

$$r_i^2 = \frac{I_i}{A_i L_i^2}. \tag{5c}$$

After decoupling the functions $Y_i(\xi_i)$ and $L_i\Psi_i(\xi_i)$ in ((3)-(4)), the decoupled fourth-order differential equations in the nondimensional form can be written as

$$Y_i''''(\xi_i) + \alpha_i Y_i''(\xi_i) + \beta_i^2 Y_i(\xi_i) = 0, \tag{6}$$

$$L_i\Psi_i''''(\xi_i) + \alpha_i L_i \Psi_i''(\xi_i) + \beta_i^2 L_i \Psi_i(\xi_i) = 0, \tag{7}$$

where

$$\alpha_i = \lambda_i^4\left(r_i^2 + s_i^2\right), \tag{7a}$$

$$\beta_i^2 = \lambda_i^4\left(\lambda_i^4 r_i^2 s_i^2 - 1\right). \tag{7b}$$

The general solution of (6) and (7) can be written, respectively, in the form

$$\begin{aligned}Y_i(\xi_i) &= C_{1i}\sin(a_i\xi_i) + C_{2i}\cos(a_i\xi_i)\\&\quad + C_{3i}\sinh(b_i\xi_i) + C_{4i}\cosh(b_i\xi_i),\\ L_i\Psi_i(\xi_i) &= -\left(\frac{\delta_{1i}}{a_i}\right)C_{1i}\cos(a_i\xi_i)\\&\quad + \left(\frac{\delta_{1i}}{a_i}\right)C_{2i}\sin(a_i\xi_i)\\&\quad + \left(\frac{\delta_{2i}}{b_i}\right)C_{3i}\cosh(b_i\xi_i)\\&\quad + \left(\frac{\delta_{2i}}{b_i}\right)C_{4i}\sinh(b_i\xi_i).\end{aligned} \tag{8}$$

Here,

$$a_i^2 = \left(\frac{\alpha_i}{2}\right) + \sqrt{\left(\frac{\alpha_i}{2}\right)^2 - \beta_i^2}, \tag{9a}$$

$$b_i^2 = -\left(\frac{\alpha_i}{2}\right) + \sqrt{\left(\frac{\alpha_i}{2}\right)^2 - \beta_i^2}. \tag{9b}$$

One can derive the expressions of δ_{1i} and δ_{2i} using (8), together with (3) or (4) in the form

$$\delta_{1i} = s_i^2 \lambda_i^4 - a_i^2, \tag{10a}$$

$$\delta_{2i} = s_i^2 \lambda_i^4 + b_i^2. \tag{10b}$$

Here i denotes the ith span, $i = 1, 2, \ldots, n$ in the case of multispan model.

In order to introduce the current analysis, the linearly independent fundamental solutions $SY_{1i}(\xi), SY_{2i}(\xi), SY_{3i}(\xi), SY_{4i}(\xi)$ and the corresponding $S\Psi_{1i}(\xi), S\Psi_{2i}(\xi), S\Psi_{3i}(\xi), S\Psi_{4i}(\xi)$ are derived. In order to simplify the solution of Timoshenko beam, the following dependent functions are defined:

$$\Gamma_i(\xi) = Y_i'(\xi) - L_i \Psi_i(\xi), \tag{11a}$$

$$S\Gamma_{1i}(\xi) = SY_{1i}'(\xi) - S\Psi_{1i}(\xi), \tag{11b}$$

$$S\Gamma_{2i}(\xi) = SY_{2i}'(\xi) - S\Psi_{2i}(\xi), \tag{11c}$$

$$S\Gamma_{3i}(\xi) = SY_{3i}'(\xi) - S\Psi_{3i}(\xi), \tag{11d}$$

$$S\Gamma_{4i}(\xi) = SY_{4i}'(\xi) - S\Psi_{4i}(\xi). \tag{11e}$$

The Timoshenko solution will be normalized at the origin of coordinates as follows:

$$\begin{bmatrix} SY_{1i}(0) & S\Psi_{1i}(0) & S\Psi_{1i}'(0) & S\Gamma_{1i}(0) \\ SY_{2i}(0) & S\Psi_{2i}(0) & S\Psi_{2i}'(0) & S\Gamma_{2i}(0) \\ SY_{3i}(0) & S\Psi_{3i}(0) & S\Psi_{3i}'(0) & S\Gamma_{3i}(0) \\ SY_{4i}(0) & S\Psi_{4i}(0) & S\Psi_{4i}'(0) & S\Gamma_{4i}(0) \end{bmatrix} = \begin{bmatrix} 1 & 0 & 0 & 0 \\ 0 & 1 & 0 & 0 \\ 0 & 0 & 1 & 0 \\ 0 & 0 & 0 & 1 \end{bmatrix}. \tag{12}$$

Substituting the general solution of (8) in each raw in (12) we get the following set of fundamental solutions:

$$SY_{1i}(\xi_i) = \frac{1}{\delta_{1i} - \delta_{2i}} \left(-\delta_{2i} \cos(a_i \xi_i) + \delta_{1i} \cosh(b_i \xi_i)\right), \tag{13a}$$

$$SY_{2i}(\xi_i) = \frac{1}{\left(\delta_{2i} a_i^2 + \delta_{1i} b_i^2\right)} \left(a_i \left(\delta_{2i} - b_i^2\right) \sin(a_i \xi_i) + b_i \left(\delta_{1i} + a_i^2\right) \sinh(b_i \xi_i)\right), \tag{13b}$$

$$SY_{3i}(\xi_i) = \frac{1}{\delta_{1i} - \delta_{2i}} \left(\cos(a_i \xi_i) - \cosh(b_i \xi_i)\right), \tag{13c}$$

$$SY_{4i}(\xi_i) = \frac{1}{\left(\delta_{2i} a_i^2 + \delta_{1i} b_i^2\right)} \left(\delta_{2i} a_i \sin(a_i \xi_i) + \delta_{1i} b_i \sinh(b_i \xi_i)\right), \tag{13d}$$

$$S\Psi_{1i}(\xi_i) = \frac{\delta_{1i} \delta_{2i}}{\delta_{1i} - \delta_{2i}} \left(-\frac{1}{a_i} \sin(a_i \xi_i) + \frac{1}{b_i} \sinh(b_i \xi_i)\right), \tag{13e}$$

$$S\Psi_{2i}(\xi_i) = \frac{1}{\left(\delta_{2i} a_i^2 + \delta_{1i} b_i^2\right)} \left(-\delta_{1i} \left(\delta_{2i} - b_i^2\right) \cos(a_i \xi_i) + \delta_{2i} \left(\delta_{1i} + a_i^2\right) \cosh(b_i \xi_i)\right), \tag{13f}$$

$$S\Psi_{3i}(\xi_i) = \frac{1}{\delta_{1i} - \delta_{2i}} \left(\frac{\delta_{1i}}{a_i} \sin(a_i \xi_i) - \frac{\delta_{2i}}{b_i} \sinh(b_i \xi_i)\right), \tag{13g}$$

$$S\Psi_{4i}(\xi_i) = \frac{\delta_{1i} \delta_{2i}}{\left(\delta_{2i} a_i^2 + \delta_{1i} b_i^2\right)} \left(-\cos(a_i \xi_i) + \cosh(b_i \xi_i)\right). \tag{13h}$$

The general solution of the beam can be presented in terms of the set of fundamental solutions as

$$\begin{aligned} Y_i(\xi_i) &= y_{i0} SY_{1i}(\xi_i) + \psi_{i0} SY_{2i}(\xi_i) + \psi_{i0}' SY_{3i}(\xi_i) + \gamma_{i0} SY_{4i}(\xi_i), \\ L_i \Psi_i(\xi_i) &= y_{i0} S\Psi_{1i}(\xi_i) + \psi_{i0} S\Psi_{2i}(\xi) + \psi_{i0}' S\Psi_{3i}(\xi) + \gamma_{i0} S\Psi_{4i}(\xi_i), \\ \Gamma_i(\xi_i) &= y_{i0} S\Gamma_{1i}(\xi_i) + \psi_{i0} S\Gamma_{2i}(\xi_i) + \psi_{i0}' S\Gamma_{3i}(\xi_i) + \gamma_{i0} S\Gamma_{4i}(\xi_i), \end{aligned} \tag{14}$$

where $y_{i0} = Y_i(0)$, $\psi_{i0} = L_i \Psi_i(0)$, $\psi_{i0}' = L_i \Psi_i'(0)$, and $\gamma_{i0} = \Gamma_i(0)$.

The beam start boundary conditions at the point of attachment 1 can be presented in nondimensional form as

$$\begin{aligned} L_1 \Psi_1'(0) + \left(\overline{J}_1 \lambda_1^4 - \Phi_1\right) L_1 \Psi_1(0) = 0, \\ \Gamma_1(0) + s_1^2 \left(\overline{m}_1 \lambda_1^4 - Z_1\right) Y_1(0) = 0, \end{aligned} \tag{15}$$

where

$$\overline{J}_1 = \frac{J_1}{\rho_1 A_1 L_1^3}, \tag{16a}$$

$$\lambda_1^4 = \frac{\rho_1 A_1 L_1^4 \omega^2}{E_1 I_1}, \tag{16b}$$

$$Z_1 = \frac{k_1 L_1^3}{E_1 I_1}, \tag{16c}$$

$$\Phi_1 = \frac{\phi_1 L_1}{E_1 I_1}, \tag{16d}$$

$$\overline{m}_1 = \frac{m_1}{\rho_1 A_1 L_1}, \tag{16e}$$

where J_1 is the mass moment of inertia at station 1, k_1 and ϕ_1 are the linear and rotational elastic supports at station 1, respectively, and m_1 is the concentrated mass at station 1; see Figure 1 for details.

Substituting the solutions presented in (13a), (13b), (13c), (13d), (13e), (13f), (13g), (13h)-(14) into (15), the following equations are obtained:

$$\begin{aligned} \left(\overline{J}_1 \lambda_1^4 - \Phi_1\right) \psi_{10} + \psi'_{10} &= 0, \\ s_1^2 \left(\overline{m}_1 \lambda_1^4 - Z_1\right) y_{10} + \gamma_{10} &= 0. \end{aligned} \tag{17}$$

The start boundary conditions in (17) can be presented in matrix form as

$$\begin{bmatrix} 0 & \left(\overline{J}_1 \lambda_1^4 - \phi_1\right) & 1 & 0 \\ s_1^2 \left(\overline{m}_1 \lambda_1^4 - Z_1\right) & 0 & 0 & 1 \end{bmatrix} \begin{Bmatrix} y_{10} \\ \psi_{10} \\ \psi'_{10} \\ \gamma_{10} \end{Bmatrix} = 0. \tag{18}$$

This equation can be simply written as

$$\left[\mathbf{U}^{\mathbf{s}}\right] \{\Delta\}_1 = 0, \tag{19}$$

where

$$\{\mathbf{\Delta}\}_1 = \left\{ y_{10} \quad \psi_{10} \quad \psi'_{10} \quad \gamma_{10} \right\}^t, \tag{20}$$

where the superscript t indicates vector transpose.

At station $(n+1)$, the beam end boundary conditions can be written in the nondimensional form as

$$\begin{aligned} \Psi'_n(1) + \left(\Phi_{n+1} - \lambda_n^4 \overline{J}_{n+1}\right) \Psi_n(1) &= 0, \\ \Gamma_n(1) + \left(Z_{n+1} - \overline{m}_{n+1} \lambda_n^4\right) s_n^2 Y_n(1) &= 0, \end{aligned} \tag{21}$$

where

$$\overline{J}_{n+1} = \frac{J_{n+1}}{\rho_n A_n L_n^3}, \tag{22a}$$

$$\lambda_n^4 = \frac{\rho_n A_n L_n^4 \omega^2}{E_n I_n}, \tag{22b}$$

$$Z_{n+1} = \frac{k_{n+1} L_n^3}{E_n I_n}, \tag{22c}$$

$$\Phi_{n+1} = \frac{\phi_{n+1} L_n}{E_n I_n}, \tag{22d}$$

$$\overline{m}_{n+1} = \frac{m_{n+1}}{\rho_n A_n L_n}, \tag{22e}$$

where J_{n+1} is the mass moment of inertia at station $(n+1)$, k_{n+1} and ϕ_{n+1} are the linear and rotational elastic supports at station $(n+1)$, respectively, and m_{n+1} is the concentrated mass at station $(n+1)$.

Substituting the solutions in (13a), (13b), (13c), (13d), (13e), (13f), (13g), (13h)-(14) into (21), the following equations are obtained:

$$\begin{aligned} & y_{n0} \left(S\Psi'_{1n}(1) + \left(\Phi_{n+1} - \lambda_n^4 \overline{J}_{n+1}\right) S\Psi_{1n}\right) \\ & \quad + \psi_{n0} \left(S\Psi'_{2n}(1) + \left(\Phi_{n+1} - \lambda_n^4 \overline{J}_{n+1}\right) S\Psi_{2n}\right) \\ & \quad + \psi'_{n0} \left(S\Psi'_{3n}(1) + \left(\Phi_{n+1} - \lambda_n^4 \overline{J}_{n+1}\right) S\Psi_{3n}\right) \\ & \quad + \gamma_{n0} \left(S\Psi'_{4n}(1) + \left(\Phi_{n+1} - \lambda_n^4 \overline{J}_{n+1}\right) S\Psi_{4n}\right) = 0, \\ & y_{n0} \left(S\Gamma_{1n}(1) + s_n^2 \left(Z_{n+1} - \overline{m}_{n+1} \lambda_n^4\right) SY_{1n}(1)\right) \\ & \quad + \psi_{n0} \left(S\Gamma_{2n}(1) + s_n^2 \left(Z_{n+1} - \overline{m}_{n+1} \lambda_n^4\right) SY_{2n}(1)\right) \\ & \quad + \psi'_{n0} \left(S\Gamma_{3n}(1) + s_n^2 \left(Z_{n+1} - \overline{m}_{n+1} \lambda_n^4\right) SY_{3n}(1)\right) \\ & \quad + \gamma_{n0} \left(S\Gamma_{4n}(1) + s_n^2 \left(Z_{n+1} - \overline{m}_{n+1} \lambda_n^4\right) SY_{4n}(1)\right) \\ & \quad = 0. \end{aligned} \tag{23}$$

Equation (23) can be written in the matrix form as

$$\begin{bmatrix} \left(S\Psi'_{1n}(1) + \left(\Phi_{n+1} - \lambda_n^4 \overline{J}_{n+1}\right) S\Psi_{1n}\right) & \left(S\Psi'_{2n}(1) + \left(\Phi_{n+1} - \lambda_n^4 \overline{J}_{n+1}\right) S\Psi_{2n}\right) & \left(S\Psi'_{3n}(1) + \left(\Phi_{n+1} - \lambda_n^4 \overline{J}_{n+1}\right) S\Psi_{3n}\right) & \left(S\Psi'_{4n}(1) + \left(\Phi_{n+1} - \lambda_n^4 \overline{J}_{n+1}\right) S\Psi_{4n}\right) \\ \left(S\Gamma_{1n}(1) + s_n^2 \left(Z_{n+1} - \overline{m}_{n+1} \lambda_n^4\right) SY_{1n}(1)\right) & \left(S\Gamma_{2n}(1) + s_n^2 \left(Z_{n+1} - \overline{m}_{n+1} \lambda_n^4\right) SY_{2n}(1)\right) & \left(S\Gamma_{3n}(1) + s_n^2 \left(Z_{n+1} - \overline{m}_{n+1} \lambda_n^4\right) SY_{3n}(1)\right) & \left(S\Gamma_{4n}(1) + s_n^2 \left(Z_{n+1} - \overline{m}_{n+1} \lambda_n^4\right) SY_{4n}(1)\right) \end{bmatrix} \begin{Bmatrix} y_{n0} \\ \psi_{n0} \\ \psi'_{n0} \\ \gamma_{n0} \end{Bmatrix} = 0. \tag{24}$$

This equation can be simply written as

$$\left[\mathbf{U}^{\mathbf{E}}\right]_{2\times 4} \{\Delta\}_n = 0, \tag{25}$$

where

$$\{\mathbf{\Delta}\}_n = \left\{ y_{n0} \quad \psi_{n0} \quad \psi'_{n0} \quad \gamma_{n0} \right\}^t. \tag{26}$$

The beam intermediate continuity conditions can be presented in nondimensional form as

$$Y_i(1) = Y_{i+1}(0),$$

$$L_{(i+1)i} L_i \Psi_i(1) = L_{(i+1)} \Psi_{i+1}(0),$$

$$
\begin{aligned}
&(EI)_{i(i+1)} * L^2_{(i+1)i}\left(\Psi_i'(1) + \left(\Phi_{i+1} - \overline{J}_{i+1}\lambda_i^4\right)\Psi_i(1)\right)\\
&\quad = L_{(i+1)}\Psi_{i+1}'(0),\\
&\left(k'GA\right)_{i(i+1)} L_{(i+1)i}\left(\Gamma_i(1) + s_i^2\left(Z_{i+1} - m_{i+1}\lambda_i^4\right)Y_i(1)\right)\\
&\quad = \Gamma_{i+1}(0),
\end{aligned}
\tag{27}
$$

where

$$\overline{J}_{i+1} = \frac{J_{i+1}}{\rho_i A_i L_i^3}, \tag{28a}$$

$$\lambda_i^4 = \frac{\rho_i A_i L_i^4 \omega^2}{E_i I_i}, \tag{28b}$$

$$Z_{i+1} = \frac{k_{i+1} L_i^3}{E_i I_i}, \tag{28c}$$

$$\Phi_{i+1} = \frac{\phi_{i+1} L_i}{E_i I_i}, \tag{28d}$$

$$\overline{m}_{i+1} = \frac{m_{i+1}}{\rho_i A_i L_i}, \tag{28e}$$

where J_{i+1} is the mass moment of inertia at station $(i+1)$, k_{i+1} and ϕ_{i+1} are the linear and rotational stiffness at station $(i+1)$, respectively, and m_{i+1} is the concentrated mass at station $(i+1)$.

Substituting the solutions in (13a), (13b), (13c), (13d), (13e), (13f), (13g), (13h)-(14) into (27), we get the following equations:

$$
\begin{aligned}
y_{(i+1)0} &= y_{i0} SY_{1i}(1) + \psi_{i0} SY_{2i}(1) + \psi_{i0}' SY_{3i}(1)\\
&\quad + \gamma_{i0} SY_{4i}(1),\\
\psi_{(i+1)0} &= L_{(i+1)i}\left(y_{i0} S\Psi_{1i}(1) + \psi_{i0} S\Psi_{2i}(1)\right.\\
&\quad \left. + \psi_{i0}' S\Psi_{3i}(1) + \gamma_{i0} S\Psi_{4i}(1)\right),\\
\psi_{(i+1)0}' &= (EI)_{i(i+1)} * L^2_{(i+1)i}\left(y_{i0}\left(S\Psi_{1i}'(1)\right.\right.\\
&\quad + \left(\Phi_{i+1} - \overline{J}_{i+1}\lambda_i^4\right) S\Psi_{1i}(1)\Big) + \psi_{i0}\left(S\Psi_{2i}'(1)\right.\\
&\quad \left. + \left(\Phi_{i+1} - \overline{J}_{i+1}\lambda_i^4\right) S\Psi_{2i}(1)\right) + \psi_{i0}'\left(S\Psi_{3i}'(1)\right.\\
&\quad \left. + \left(\Phi_{i+1} - \overline{J}_{i+1}\lambda_i^4\right) S\Psi_{3i}(1)\right) + \gamma_{i0}\left(S\Psi_{4i}'(1)\right.\\
&\quad \left.\left. + \left(\Phi_{i+1} - \overline{J}_{i+1}\lambda_i^4\right) S\Psi_{4i}(1)\right)\right),\\
\gamma_{(i+1)0} &= \left(k'GA\right)_{i(i+1)} L_{(i+1)i}\left(y_{i0}\left(S\Gamma_{1i}(1)\right.\right.\\
&\quad + s_i^2\left(Z_{i+1} - m_{i+1}\lambda_i^4\right) SY_{1i}(1)\Big) + \psi_{i0}\left(S\Gamma_{2i}(1)\right.\\
&\quad \left. + s_i^2\left(Z_{i+1} - m_{i+1}\lambda_i^4\right) SY_{2i}(1)\right) + \psi_{i0}'\left(S\Gamma_{3i}(1)\right.\\
&\quad \left. + s_i^2\left(Z_{i+1} - m_{i+1}\lambda_i^4\right) SY_{3i}(1)\right) + \gamma_{i0}\left(S\Gamma_{4i}(1)\right.\\
&\quad \left.\left. + s_i^2\left(Z_{i+1} - m_{i+1}\lambda_i^4\right) SY_{4i}(1)\right)\right).
\end{aligned}
\tag{29}
$$

Equation (29) can be written in matrix form as

$$
\begin{bmatrix}
SY_{1i}(1) & SY_{2i}(1) & SY_{3i}(1) & SY_{4i}(1)\\
L_{(i+1)i} S\Psi_{1i}(1) & L_{(i+1)i} S\Psi_{2i}(1) & L_{(i+1)i} S\Psi_{3i}(1) & L_{(i+1)i} S\Psi_{4i}(1)\\
W_{1i}\left(S\Psi_{1i}'(1) + \left(\Phi_{i+1} - \overline{J}_{i+1}\lambda_i^4\right) S\Psi_{1i}(1)\right) & W_{1i}\left(S\Psi_{2i}'(1) + \left(\Phi_{i+1} - \overline{J}_{i+1}\lambda_i^4\right) S\Psi_{2i}(1)\right) & W_{1i}\left(S\Psi_{3i}'(1) + \left(\Phi_{i+1} - \overline{J}_{i+1}\lambda_i^4\right) S\Psi_{3i}(1)\right) & W_{1i}\left(S\Psi_{4i}'(1) + \left(\Phi_{i+1} - \overline{J}_{i+1}\lambda_i^4\right) S\Psi_{4i}(1)\right)\\
W_{2i}\left(S\Gamma_{1i}(1) + s_i^2\left(Z_{i+1} - m_{i+1}\lambda_i^4\right) SY_{1i}(1)\right) & W_{2i}\left(S\Gamma_{2i}(1) + s_i^2\left(Z_{i+1} - m_{i+1}\lambda_i^4\right) SY_{2i}(1)\right) & W_{2i}\left(S\Gamma_{3i}(1) + s_i^2\left(Z_{i+1} - m_{i+1}\lambda_i^4\right) SY_{3i}(1)\right) & W_{2i}\left(S\Gamma_{4i}(1) + s_i^2\left(Z_{i+1} - m_{i+1}\lambda_i^4\right) SY_{4i}(1)\right)
\end{bmatrix}
\begin{Bmatrix} y_{i0}\\ \psi_{i0}\\ \psi_{i0}'\\ \gamma_{i0} \end{Bmatrix}
= \begin{Bmatrix} y_{(i+1)0}\\ \psi_{(i+1)0}\\ \psi_{(i+1)0}'\\ \gamma_{(i+1)0} \end{Bmatrix},
\tag{30}
$$

where

$$W_{1i} = (EI)_{i(i+1)} * L^2_{(i+1)i}, \tag{31a}$$

$$W_{2i} = \left(k'GA\right)_{i(i+1)} L_{(i+1)i}. \tag{31b}$$

Equation (30) can be presented as

$$[\mathbf{T}]_{i4\times4} * \{\mathbf{\Delta}\}_i = \{\mathbf{\Delta}\}_{i+1}, \tag{32}$$

where

$$\{\mathbf{\Delta}\}_i = \left\{y_{i0} \;\; \psi_{i0} \;\; \psi_{i0}' \;\; \gamma_{i0}\right\}^t, \tag{33a}$$

$$\{\mathbf{\Delta}\}_{i+1} = \left\{y_{(i+1)0} \;\; \psi_{(i+1)0} \;\; \psi_{(i+1)0}' \;\; \gamma_{(i+1)0}\right\}^t. \tag{33b}$$

From (32), one can find that

$$\{\mathbf{\Delta}\}_n = [\mathbf{T}]_{n-1}\{\mathbf{\Delta}\}_{n-1} = [\mathbf{T}]_{n-1}[\mathbf{T}]_{n-2}\cdots[\mathbf{T}]_2\{\mathbf{\Delta}\}_1. \tag{34}$$

The intermediate spans transfer matrix can be presented as

$$[\mathbf{T}]_{4\times4} = [\mathbf{T}]_{n-1}[\mathbf{T}]_{n-2}\cdots[\mathbf{T}]_2; \tag{35}$$

then (34) can be presented as

$$\{\mathbf{\Delta}\}_n = [\mathbf{T}]_{4\times4}\{\mathbf{\Delta}\}_1. \tag{36}$$

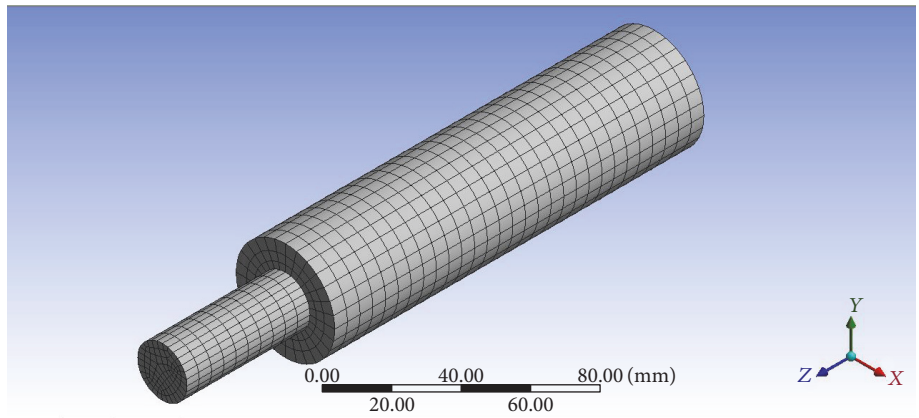

Figure 2: Finite element 3D mesh.

Substituting (36) into the end condition of (25) results in the following equations:

$$\left[\mathbf{U^E}\right]_{2\times4}[\mathbf{T}]_{4\times4}\{\Delta\}_1 = 0, \tag{37}$$

$$\left[\mathbf{U^{IE}}\right]_{2\times4} = \left[\mathbf{U^E}\right]_{2\times4}[\mathbf{T}]_{4\times4}, \tag{38}$$

$$\left[\mathbf{U^{IE}}\right]_{2\times4}\{\Delta\}_1 = 0. \tag{39}$$

The general beam equation can be presented using the start boundary condition in (19) and the beam intermediate and end condition in (39) as shown below

$$\left[\mathbf{U^{tot}}\right]_{4\times4}\{\Delta\}_1 = 0, \tag{40}$$

where

$$\left[\mathbf{U^{tot}}\right]_{4\times4} = \begin{bmatrix}\left[\mathbf{U^S}\right]_{2\times4}\\ \left[\mathbf{U^{IE}}\right]_{2\times4}\end{bmatrix}. \tag{41}$$

Equating the determinant of $[\mathbf{U^{tot}}]$ by zero results in the system frequency equation. In general, the TMM has advantages over the traditional methods in that the final frequency equation is 4×4 for any number of beam segments. The advantage of the current method NTM over the TMM is significant in the using of tailored solution that is normalized at the origin of coordinates. This type of solution enables the formulation of the system equations without the need to any inverse matrix procedures as shown previously. This reduces the computational time comparing with the TMM.

2.2. Finite Element Method. Among the numerical tools, finite element method is considered one of most efficient methods to perform the vibration analysis of mechanical and structural components. In this section, finite element is used to obtain the natural frequencies and mode shapes of uniform and stepped beams. ANSYS finite element commercial package is used to perform the finite element analysis. The analysis is done using three-dimensional (3D) solid element models and SOLID95 elements are used for meshing. Since all the experimentally investigated samples in the current work are round and stepped. The beam cross-section is free meshed using 87 SOLID95 elements for smaller cross-section and 171 elements for the larger cross-section. This mesh is then extruded using 40 elements along the length of the beam. The total number of the element is ranging from 3480 (40×87) to 6840 (40×171) elements based on the location of the step; see Figure 2. Modal analysis module is used in this analysis and Block Lanczos method is used for the mode extraction method. The finite element model FE(3D) results are compared with those obtained experimentally and analytically.

3. Results and Discussion

3.1. Verification and Validation of NTM Results

3.1.1. Verification Example 1. In this example, the first five nondimensional natural frequencies ($\lambda_i^{*4} = \rho_1 A_1 L^4 \omega^2 / E_1 I_1$) of stepped beam are compared with the exact solution presented by Gutierrez et al. [18]; see Figure 3. The model is solved at two different step locations and several values of b_{21} and h_{21} as shown in Table 1. Three different values of rotary inertia $r_1^2 = vs, 0.0036$ and 0.01 are considered in order to validate the current model in case of Bernoulli-Euler and Timoshenko beams. The value of $s_1^2 = 3.12 r_1^2$ is considered in order to evaluate the shear deformation [18]. The values of nondimensional linear and rotational elastic supports stiffness at start and the end are ($Z_1 = 10, \Phi_1 = vl$), ($Z_3 = vs, \Phi_3 = vl$), respectively. The results of Table 1 show that the present NTM results are in good agreement with the exact solution presented by Gutierrez et al. [18].

3.1.2. Verification Example 2. In this example, Timoshenko beam with three-step round cross-section presented in [19] is investigated; see Figure 4. An intermediate lumped mass of $m_3^* = m_3 / \rho_1 A_1 L = 1$ is located at a distance of 750 mm from point 1. The input data for this example is listed in the caption of Figure 4. Table 2 shows the results of the first five natural frequencies ω_i in (rad/sec) for pinned-pinned, free-clamped, clamped-free, clamped-pinned, and clamped-clamped configurations. The results of reference [19] are

Table 1: The first five natural frequencies λ_i^{*2} for stepped Timoshenko beam in the case where the beam is rigidly restrained against rotation $\phi_1^* = vl$ and elastically restrained in translation $Z_1^* = 10$ in comparison with [18].

r_1^2	μ	b_{21}	h_{21}	λ_1^{*2}	λ_2^{*2}	λ_3^{*2}	λ_4^{*2}	λ_5^{*2}
10^{-7}								
[18]	0.25	1.0	0.8	3.010	9.696	34.010	74.430	132.341
Present NTM				3.0098	9.6956	34.0101	74.4300	132.3410
[18]		0.8	0.8	3.249	9.664	34.315	74.645	131.803
Present NTM				3.2490	9.6638	34.3151	74.6445	131.7507
[18]		0.8	0.6	3.385	8.117	28.630	60.997	103.439
Present NTM				3.3851	8.1171	28.6302	60.9947	103.4075
[18]	0.50	1.0	0.8	2.958	10.046	34.993	80.145	139.666
Present NTM				2.9579	10.0460	34.9931	80.1455	139.6667
[18]		0.8	0.8	3.124	10.165	34.688	80.570	139.175
Present NTM				3.1240	10.1655	34.6882	80.5707	139.1759
[18]		0.8	0.6	3.284	9.499	28.501	70.123	118.482
Present NTM				3.2841	9.4989	28.5006	70.1232	118.4830
0.0036								
[18]	0.25	1.0	0.8	3.007	9.668	33.571	72.393	126.111
Present NTM				3.0066	9.6678	33.5711	72.3926	126.1107
[18]		0.8	0.8	3.245	9.635	33.862	72.607	125.617
Present NTM				3.2454	9.6354	33.8621	72.6068	125.6169
[18]		0.8	0.6	3.381	8.103	28.364	59.839	100.245
Present NTM				3.3812	8.1031	28.3643	59.8385	100.2447
[18]	0.50	1.0	0.8	2.946	9.919	33.205	71.469	116.725
Present NTM				2.9462	9.9192	33.2046	71.4693	116.7245
[18]		0.8	0.8	3.112	10.030	32.926	71.741	116.362
Present NTM				3.1120	10.0304	32.9259	71.7415	116.3618
[18]		0.8	0.6	3.272	9.391	27.449	64.020	102.697
Present NTM				3.2721	9.3908	27.4490	64.0200	102.6966
0.01								
[18]	0.25	1.0	0.8	3.001	9.619	32.841	69.229	117.238
Present NTM				3.0009	9.6192	32.8407	69.2292	117.2380
[18]		0.8	0.8	3.239	9.586	33.109	69.444	116.798
Present NTM				3.2390	9.5858	33.1092	69.4435	116.7981
[18]		0.8	0.6	3.374	8.078	27.914	57.970	95.370
Present NTM				3.3744	8.0784	27.9139	57.9705	95.3698
[18]	0.50	1.0	0.8	2.926	9.710	30.711	61.768	95.623
Present NTM				2.9255	9.7104	30.7111	61.7680	95.6230
[18]		0.8	0.8	3.019	9.809	30.464	61.912	95.326
Present NTM				3.0908	9.8086	30.4643	61.9117	95.3257
[18]		0.8	0.6	3.251	9.211	25.893	56.578	86.647
Present NTM				3.2511	9.2111	25.8933	56.5776	86.6473

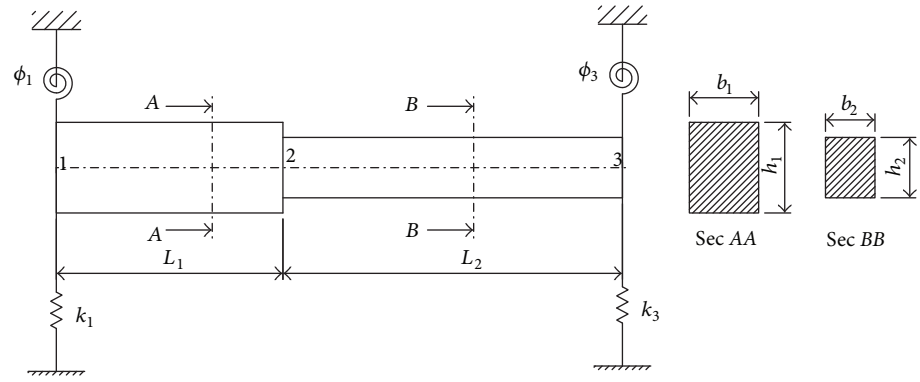

Figure 3: Verification Example 1 [18], two-span stepped beam.

Table 2: Comparison of the first five natural frequencies, in rad/sec, using the present NTM results with those obtained in [19] for the example shown in Figure 4.

	ω_n (rad/sec)	Method	Bernoulli-Euler $r_1^{*2} = 0$	Timoshenko $r_1^{*2} \neq 0$
Pinned-pinned (P-P)	ω_1	NAT [19]	319.4341	316.5288
		NTM	319.4340	316.4855
	ω_2	NAT [19]	1853.3864	1789.4207
		NTM	1853.3864	1784.8723
	ω_3	NAT [19]	4110.1341	3825.8438
		NTM	4110.1341	3836.5347
	ω_4	NAT [19]	7709.5714	6642.9094
		NTM	7709.5712	6639.2170
	ω_5	NAT [19]	11621.7699	9886.6243
		NTM	11621.7698	9918.8328
Free-clamped (F-C)	ω_1	NAT [19]	371.5354	367.9440
		NTM	371.5354	367.1487
	ω_2	NAT [19]	1243.9063	1216.6220
		NTM	1243.9065	1211.5531
	ω_3	NAT [19]	3082.0846	2827.0352
		NTM	3082.0845	2849.1465
	ω_4	NAT [19]	5541.1410	4957.9240
		NTM	5541.1409	5003.7433
	ω_5	NAT [19]	9599.3810	7673.7578
		NTM	9599.3810	7751.3336
Clamped-free (C-F)	ω_1	NTM	55.1257	55.0130
	ω_2	NTM	616.6018	598.5917
	ω_3	NTM	2702.3238	2532.1483
	ω_4	NTM	5483.2379	4969.1659
	ω_5	NTM	9570.9586	7956.5299
Clamped-pinned (C-P)	ω_1	NTM	480.8915	469.8444
	ω_2	NTM	2098.0556	1991.9611
	ω_3	NTM	5007.3315	4589.5676
	ω_4	NTM	8366.8073	7049.5393
	ω_5	NTM	13678.7112	11215.0349
Clamped-clamped (C-C)	ω_1	NTM	836.3527	807.0997
	ω_2	NTM	3019.5886	2772.2732
	ω_3	NTM	5583.6469	4980.5538
	ω_4	NTM	9625.8943	7734.8319
	ω_5	NTM	14403.3163	11538.1581

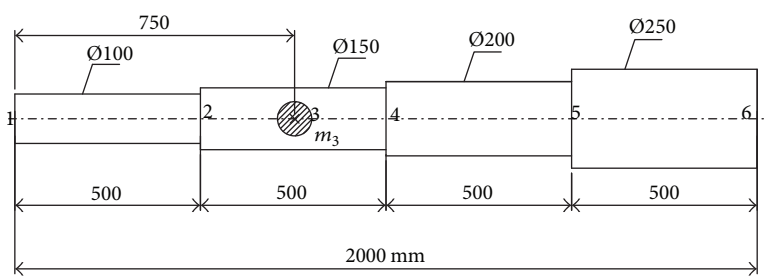

Figure 4: Verification Example 2 [19], three-step beam having $E = 206.9$ GPa. $\rho = 7836.9$ kg/m^3, $G = 79.5769$ GPa, and $k' = 0.75$.

Table 3: Comparison of the present NTM results with those obtained in [5, 20], for F-F beam shown in Figure 5.

Mode number	DQEM [20]	Exp. [5]	NTM (40)	FE(3D)	% error
	I	II	III	IV	(II & IV)
1	292.440	291	290.316	290.120	0.302
2	1181.300	1165	1162.158	1167.100	−0.180
3	1804.100	1771	1767.321	1772.200	−0.068

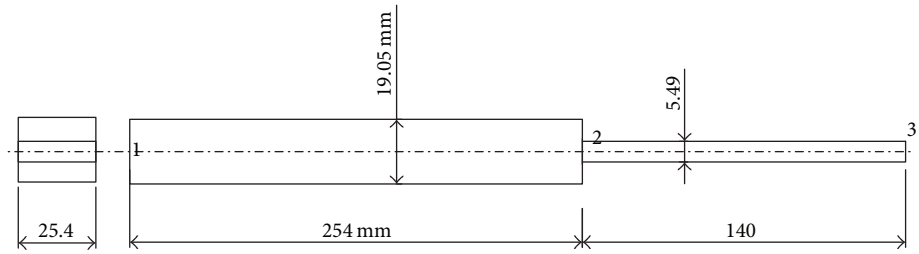

Figure 5: Verification Example 3 [5, 20], single-step (F-F) aluminum beam having, $E = 71.7$ GPa, $\rho = 2830$ Kg/m^3, and $\nu = 0.33$.

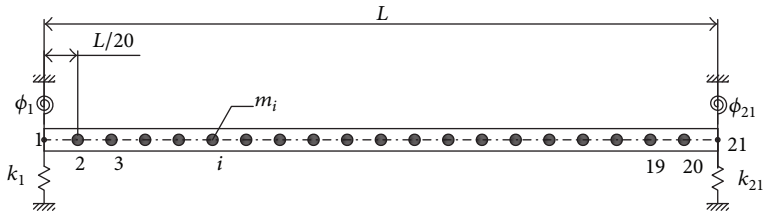

Figure 6: Verification Example 4, twenty equal span uniform beams carrying equally spaced nineteen concentrated masses with general end flexibilities conditions.

calculated using two methods. The first method is numerical assembly technique (NAT) and this method is the exact solution. The second method is differential transformation method and this method is approximate method. The pinned-pinned and free-clamped boundary conditions results are found in [19]. The results of the current analysis are in good agreement with the results presented in [19]. As can be seen from Table 2, the rotary inertia and shear deformation reduce the modal frequency especially for higher modes. Comparing the results of the clamped-free beam with the results of the free-clamped beam shows that the natural frequency results of the clamped-free beam are lower than that of free-clamped beam. This may be explained by the fact that fixing the beam from the thinner span results in lowering of the beam stiffness.

3.1.3. Verification Example 3. The third verification example is shown in Figure 5 with identical dimensions to that used in [5, 20]. The rotary inertia and shear deformation are considered. The shear coefficient k' is calculated based on [3], keeping Poisson's' ratio $\nu = 0.33$. Table 3 shows the first three nonzero free-free (F-F) eigenvalues in Hz and in comparison with [5, 20]. The present results are computed using both numerically (40) and FE(3D) methods. The results of Table 3 show that the present analysis results are very close to the experimental results. The percentage error between the present FE(3D) results and the experimental results of [5] is less than 0.302%. This represents the importance of including the effect of rotary inertia and shear deformation.

3.1.4. Verification Example 4. The fourth example is shown in Figure 6. It is for a twenty-span uniform beam carrying 19 equally spaced concentrated masses with $m_i^* = 0.1$. Several beam start and end conditions are investigated as listed in Table 4. The results are evaluated using the present NTM method and previously published numerical assembly technique NAT [6] method. The computational time required to obtain the first three frequency parameters λ_1^*, λ_2^*, and λ_3^* using both NAT and NTM methods is calculated and listed in Table 4. Considerable reduction in computational time is observed in all the investigated cases as shown in Table 4.

3.2. Test Samples and Experimental Procedures. In order to measure the natural frequencies of the system under study, the free-free test samples were put in free oscillations by using an instrumented hammer model B and K 8202. An accelerometer model B and K 4366 is fixed to the shaft in order to capture the vibration signal. The output of the charge amplifier B and K 2635 is connected to NI 6216 data acquisition card. This card is connected to the PC and managed by Lab VIEW software. Figure 10 shows a photo of the current experimental setup. The used card settings are

Table 4: Validation of the present NTM using 20-span uniform beam with 19 equally spaced concentrated masses $m_i^* = 0.1$, ($r_1^{*2} = s_1^{*2} = vs$) in comparison with [6].

Method	Z_1^*, Φ_1^*	Z_{21}^*, Φ_{21}^*	λ_1^*	λ_2^*	λ_3^*	Computational time (sec)
NAT [6]	*vs*, *vs*	*vs*, *vs*	3.7177	6.1716	8.6392	48.17
Present NTM	*vs*, *vs*	*vs*, *vs*	3.7177	6.1716	8.6392	13.53
NAT [6]	*vl*, *vs*	*vl*, *vs*	2.3871	4.7742	7.1612	34.67
Present NTM	*vl*, *vs*	*vl*, *vs*	2.3871	4.7742	7.1612	12.14
NAT [6]	*vl*, *vl*	*vl*, *vl*	3.5941	5.9671	8.35471	40.40
Present NTM	*vl*, *vl*	*vl*, *vl*	3.5941	5.9671	8.35471	13.47
NAT [6]	10, 10	10, 10	1.5989	2.5329	4.5969	22.13
Present NTM	10, 10	10, 10	1.5989	2.5329	4.5969	10.23

Table 5: Typical samples dimension of group S2 with $\overline{d} = 0.75$ shown in Figure 7.

Group S2	(Single-step beam samples of steel rod Ø 40, L = 200 mm and $\overline{d} = 30/40$)							
	L	L_1	μ	L_2	d_1	d_2	m_t (kg)	r_1^{*2}
S2-40/40	200	40	0.2	160	40	30	1.282	0.002
S2-40/100	200	100	0.5	100	40	30	1.375	0.002
S2-40/140	200	140	0.7	60	40	30	1.541	0.002

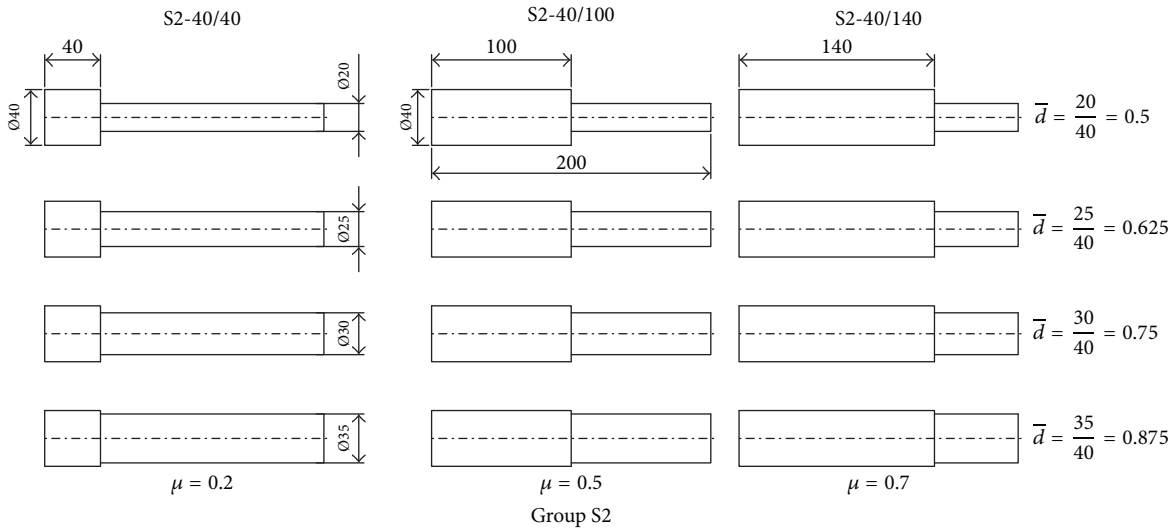

Figure 7: Schematic drawings for the experimental samples Group S2.

sample frequency of 20 kHz, sampling time of 3, 5, 8 sec, and the size of samples block to read is 1 k. The time domain data is captured and transformed into frequency domain. The resonant frequencies were obtained by the average of the results of 10 impacts applied in three different locations of the sample. Figures 7–9 show two groups of different stepped test samples, S2 and S3, respectively. All the test samples are manufactured from steel rods of dimensions Ø 80 and Ø 40 mm. The common data for the steel test samples are $\rho = 7850\,\text{kg/m}^3$, $E = 206.8\,\text{GPa}$, and $k' = 0.845$.

Two-span twelve test samples are shown in group S2, namely, S2-40/40, S2-40/100, and S2-40/140, shown in Figure 7. The dimensions of these samples are presented in Table 5. The natural frequency results of these samples are presented in Table 7 using experimental, analytical, and FE(3D) methods. The captured signal for the free vibration response for selected case from Table 7 is shown in Figure 11. This case is italicized in the table. The results of Table 7 show that the three-dimensional FE solution is closer to the experimental results than the analytical results. The maximum percentage error between the experimental and the FE results is less than 0.5%.

Group S3 consists of four different samples, namely, S3-80/250, S3-80/200, S3-80/150, and S3-80/100. More details about the geometrical dimensions and material properties for these samples are shown in Table 6 and Figure 8. The results of Table 8 show that the deviation between the FE(3D) and the experimental is less than 1.16%. The free vibration

Table 6: The sample dimensions of group S3 as shown in Figure 8.

Group S3	(Four cylindrical samples have two steps of steel rod Ø 80, L = 500 mm)							
	L	L_1	L_2	d_1	d_2	m_t (kg)	L_2^*	r_1^{*2}
S3-80/250	500	200	250	20	80	10.480	0.5	0.000100
S3-80/200	500	225	200	20	80	7.398	0.4	0.000100
S3-80/150	500	250	150	20	80	6.781	0.3	0.000100
S3-80/100	500	275	100	20	80	4.932	0.2	0.000100

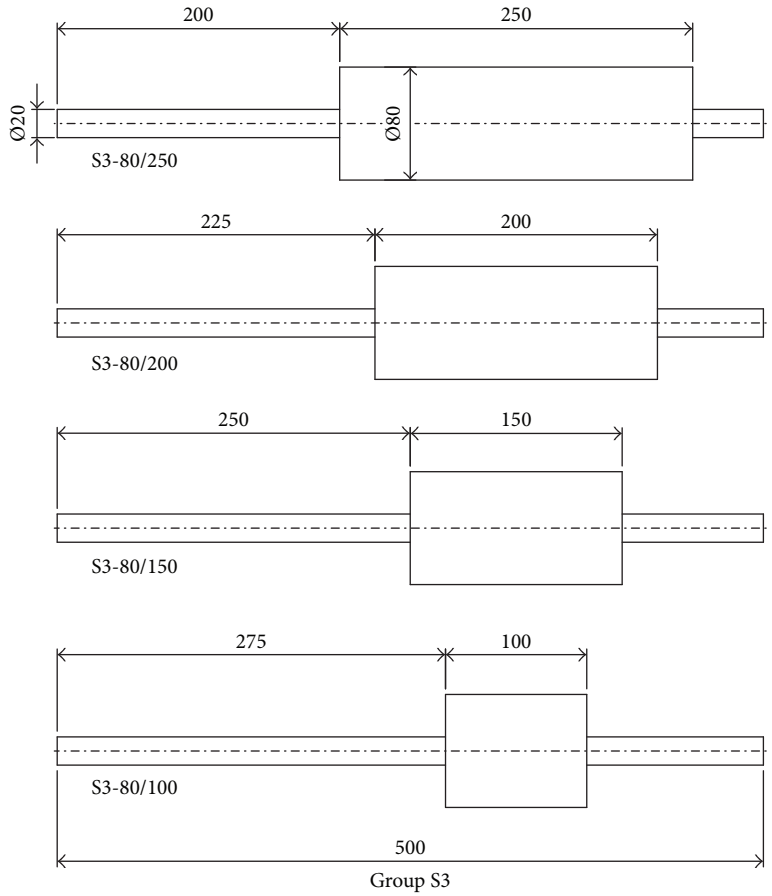

Figure 8: Schematic drawings for the experimental samples Group S3.

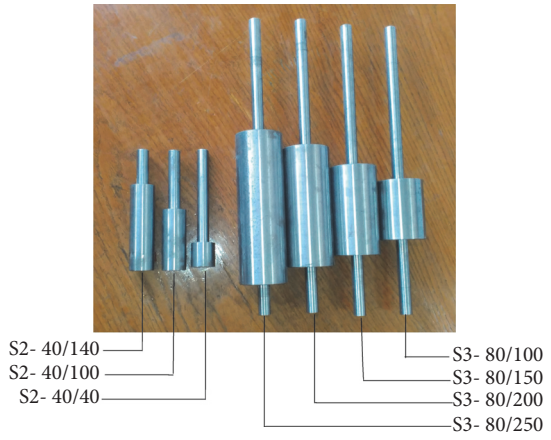

Figure 9: Real image for typical experimental test samples.

Figure 10: Test setup.

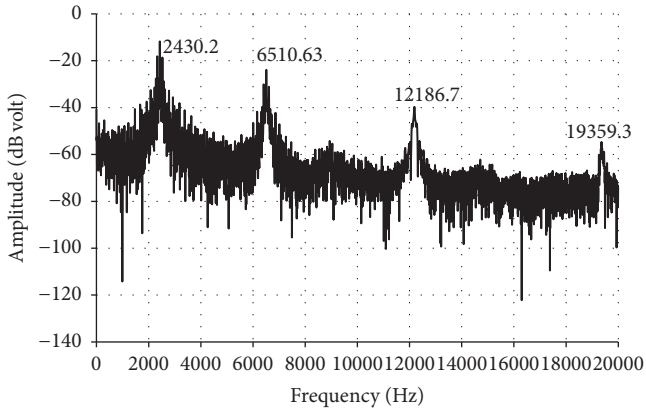

Figure 11: Experiment first four natural frequencies for test sample S2-40/40.

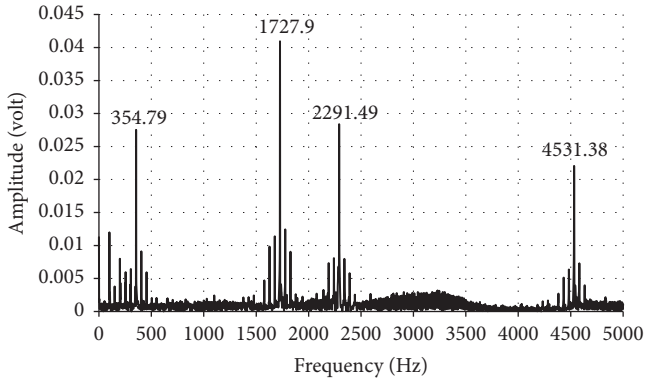

Figure 12: Experimental first four natural frequencies for test sample S3-80/200.

signals of selected case italicized in Table 8 are plotted in Figure 12. In general, the results of the three-span samples reveal the same conclusion drawn from the two-span samples that the FE(3D) results are closer to the experimental results than the analytical results. The conclusion driven from the investigated two- and three-span samples is that the three-dimensional finite element can be trusted in the prediction of the natural frequency of stepped beam.

3.3. Percentage Modal Deviation between FE(3D) and NTM Method. The results of the previous section show the accuracy of the FE(3D) model in evaluating the natural frequencies of stepped beam. Therefore, in this section, a free-free two-span model is deeply investigated using (40) and FE(3D) methods to justify the validity of the analytical solution in predicting the stepped beam results. Two categories of samples are considered as shown in Figure 13. The first category includes 600 mm length samples with $r_1^{*2} = 2.78 \times 10^{-4}$ and the second category includes 200 mm length samples with $r_1^{*2} = 205 \times 10^{-3}$. The effects of changing μ and $\overline{d}$ are investigated, μ varies from 0 to 1, and meanwhile, only three values are listed in Table 9. Four different values of $\overline{d}$ are investigated 0.5, 0.625, 0.75, and 0.875. The study in

Table 7: Percentage error between the computational and experimental results for single-step test samples (Group S2). Lowest four nonzero free-free modes.

$\overline{d}$	L_1	μ	Method	Modal frequencies in Hz			
				1	2	3	4
			(A) EXP	1848.940	5028.140	9854	16303
			(B) NTM	1873.981	5194.229	10211.79	16776.400
	40	0.2	(C) FE(3D)	1859.490	5056.749	9893.345	16380.170
			(D) % error (A, B)	1.354	3.303	3.630	2.903
			(E) % error (A, C)	0.570	0.568	0.399	0.473
			(A) EXP	2153.900	7713.530	13701.800	19845.900
			(B) NTM	2244.601	7923.127	13661.990	20230.700
20/40	100	0.5	(C) FE(3D)	2142.012	7700.169	13663.580	19793.360
			(D) % error (A, B)	4.211	2.717	−0.290	1.938
			(E) % error (A, C)	−0.551	−0.173	−0.278	−0.264
			(A) EXP	3596.820	8103.960	15773.100	20733.800
			(B) NTM	3813.426	8160.003	15739.160	21174.340
	140	0.7	(C) FE(3D)	3581.521	8090.723	15705.070	20634.360
			(D) % error (A, B)	6.022	0.691	−0.215	2.124
			(E) % error (A, C)	−0.425	−0.163	−0.431	−0.479
			(A) EXP (Figure 11)	*2430.240*	*6510.630*	*12186.700*	*19359.300*
			(B) NTM	2444.111	6638.069	12492.520	19588.580
	40	0.2	(C) FE(3D)	2430.512	6518.094	12223.080	19314.540
			(D) % error (A, B)	0.570	1.957	2.509	1.184
			(E) % error (A, C)	0.011	0.114	0.298	−0.231
			(A) EXP	2796.050	8693.500	14542.200	22134
			(B) NTM	2912.321	8781.311	14633.780	22182.430
25/40	100	0.5	(C) FE(3D)	2806.782	8698.963	14551.070	22095.920
			(D) % error (A, B)	4.158	1.010	0.629	0.218
			(E) % error (A, C)	0.383	0.062	0.060	−0.172
			(A) EXP	4015.620	8665.980	16238.9	22684
			(B) NTM	4167.385	8797.248	16074.330	22814.460
	140	0.7	(C) FE(3D)	4021.237	8655.476	16159.230	22610.690
			(D) % error (A, B)	3.779	1.514	−1.013	0.575
			(E) % error (A, C)	0.139	−0.121	−0.490	−0.323
			(A) EXP	3023.690	7906	14381.400	21856.600
			(B) NTM	3023.321	7946.457	14429.850	21806.140
	40	0.2	(C) FE(3D)	3014.442	7878.443	14307.960	21781.750
			(D) % error (A, B)	−0.012	0.511	0.336	−0.230
			(E) % error (A, C)	−0.305	−0.348	−0.510	−0.342
			(A) EXP	3401.940	9329.910	15681.400	23607.700
			(B) NTM	3478.703	9293.555	15691.770	23326.460
30/40	100	0.5	(C) FE(3D)	3405.324	9313.349	15645.690	23513.650
			(D) % error (A, B)	2.256	−0.389	0.066	−1.191
			(E) % error (A, C)	0.099	−0.177	−0.227	−0.398
			(A) EXP	4201.680	9322.630	16596.400	23967.700
			(B) NTM	4268.272	9431.643	16437.830	23729.240
	140	0.7	(C) FE(3D)	4211.100	9322.286	16530.200	23881.400
			(D) % error (A, B)	1.584	1.169	−0.955	−0.994
			(E) % error (A, C)	0.224	−0.003	−0.398	−0.360

Table 7: Continued.

$\bar{d}$	L_1	μ	Method	Modal frequencies in Hz			
				1	2	3	4
			(A) EXP	3608.280	9126.360	16128.600	23817.3
			(B) NTM	3607.895	9104.530	16000.810	23500.960
	40	0.2	(C) FE(3D)	3607.465	9106.544	16054.460	23720.110
			(D) % error (A, B)	−0.010	−0.239	−0.792	−1.328
			(E) % error (A, C)	−0.022	−0.217	−0.459	−0.408
			(A) EXP	3885.030	9778.800	16719.900	24538.800
			(B) NTM	3906.518	9705.047	16577.640	24125.780
35/40	100	0.5	(C) FE(3D)	3882.419	9759.382	16658.180	24417.41
			(D) % error (A, B)	0.553	−0.754	−0.850	−1.683
			(E) % error (A, C)	−0.067	−0.198	−0.369	−0.495
			(A) EXP	4248.240	9888.540	17028	24738.400
			(B) NTM	4253.660	9878.822	16849.850	24311.230
	140	0.7	(C) FE(3D)	4247.271	9870.286	16963.900	24616.760
			(D) % error (A, B)	0.127	−0.098	−1.046	−1.726
			(E) % error (A, C)	−0.022	−0.184	−0.376	−0.491

Table 8: Percentage error between the computational and experimental results for two-step samples (Group S3). Lowest four nonzero free-free modes.

	Method	Modal frequencies in Hz			
		1	2	3	4
S3-80/250					
	(A) EXP	403.148	2126.460	4139.830	5153.500
	(B) NTM	420.212	2203.984	4334.192	5605.556
	(C) FE(3D)	404.180	2126.900	4153.700	5169.800
	(D) % error (A, B)	−3.966	3.517	4.484	−8.428
	(E) % error (A, C)	−0.255	−0.020	−0.333	−0.315
S3-80/200					
	(A) EXP (Figure 12)	*354.790*	*1727.900*	*2291.490*	*4531.380*
	(B) NTM	367.381	1788.472	2551.555	4660.983
	(C) FE(3D)	355.230	1728.300	2318.400	4532.200
	(D) % error (A, B)	−3.549	3.386	10.192	−2.860
	(E) % error (A, C)	0.124	0.023	1.160	0.018
S3-80/150					
	(A) EXP	335.859	1360.050	1545.130	3778.200
	(B) NTM	346.243	1434.113	1638.174	3889.033
	(C) FE(3D)	336.440	1364.200	1548.500	3781.900
	(D) % error (A, B)	−3.091	−5.445	−6.021	−2.933
	(E) % error (A, C)	0.172	0.305	0.218	0.097
S3-80/100					
	(A) EXP	337.400	1018.240	1371.070	3221.200
	(B) NTM	345.942	1074.574	1424.992	3303.837
	(C) FE(3D)	337.480	1024	1372.900	3215
	(D) % error (A, B)	−2.531	−5.532	−3.932	−2.565
	(E) % error (A, C)	0.023	0.565	0.133	−0.192

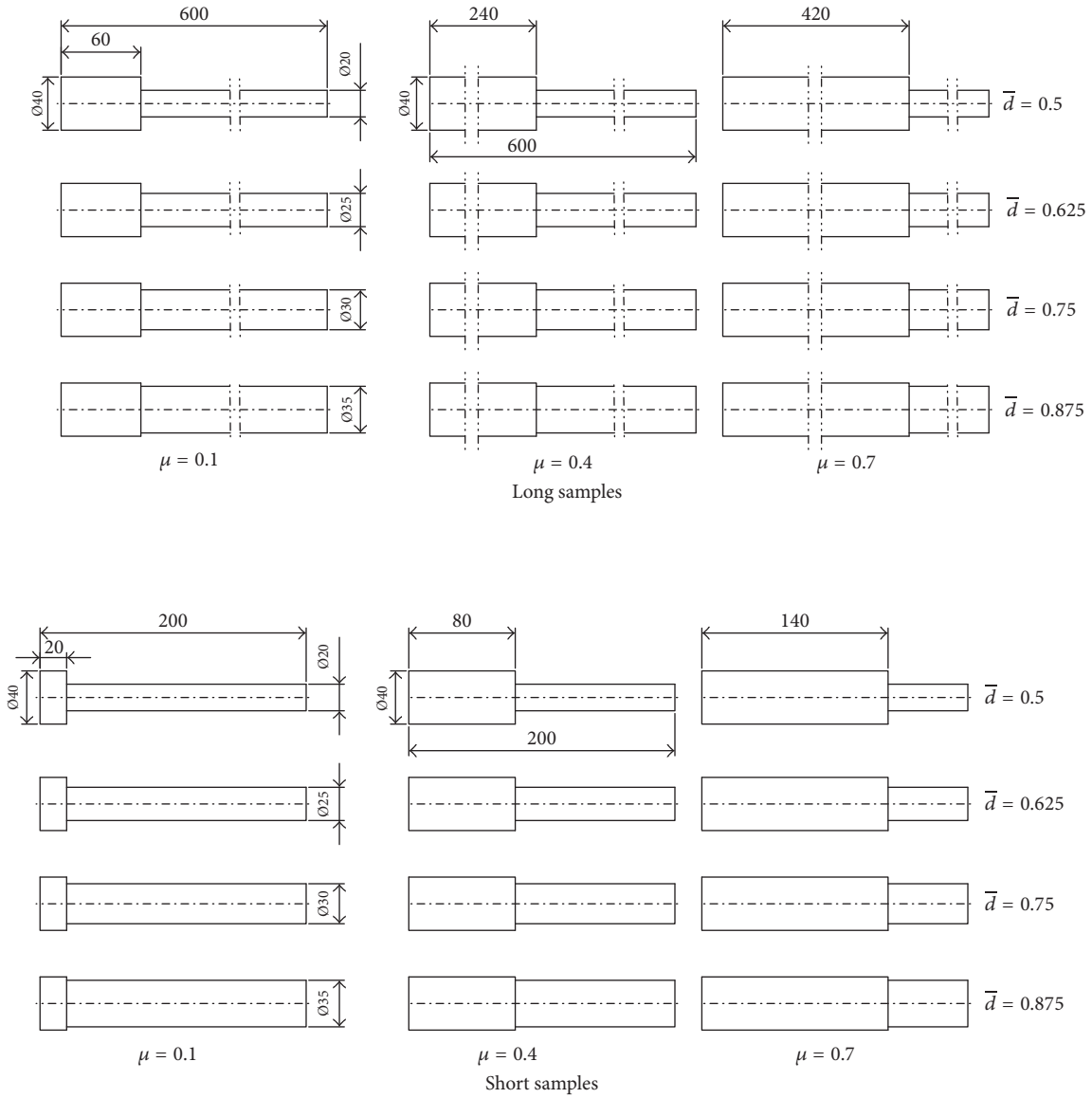

FIGURE 13: Long and short stepped samples at three values of $\mu = 0.1, 0.4,$ and 0.7 and four values of $\overline{d} = h_{21} = 0.5, 0.625, 0.75,$ and 0.875.

this section focuses only on the first three nonzero free-free modes. The percentage modal deviation in analytical NTM solution prediction in reference to the FE(3D) solution is presented in Figure 13 for long samples and in Figure 14 for short samples. This percentage deviation is calculated using the following formula:

$$\text{Dev}_i = \frac{f_{(\text{NTM})_i} - f_{(\text{FE})_i}}{f_{(\text{FE})_i}} * 100, \tag{42}$$

where

Dev_i is the percentage deviation in the ith modal frequency,

$f_{(\text{FE})_i}$ is the ith mode natural frequency using three-dimensional finite element,

$f_{(\text{NTM})_i}$ is the ith mode natural frequency using analytical NTM method.

The results of Table 9 show that, for the investigated examples with step ratio smaller than one, the increase in μ and/or $\overline{d}$ increases the modal frequencies. The percentage deviations in the analytical NTM results for the short samples are higher than those for the longer samples. The percentage deviations in the analytical natural frequency prediction are plotted for the long and short examples in Figures 14 and 15, respectively. Figures 14(a) and 15(a) present a plot for Dev_1, Figures 14(b) and 15(b) present a plot for Dev_2, and Figures 14(c) and 15(c) present a plot for Dev_3. Figure 16(a) presents the first mode shape at the conditions of the peak point in Figure 15(a), Figure 16(b) presents the second mode shape at the conditions of the peak point in Figure 15(b), and Figure 16(c) presents the third mode shape at the conditions of the peak point in Figure 15(c).

Figures 14(a) and 15(a) show that, for long and short stepped samples, the Dev_1 attains the peak when μ lies

Table 9: Typical relative deviation between present NTM and finite element (3D) results. Lowest three nonzero modes for two categories of single-step F-F beam; see Figure 13.

$\overline{d}$	Method	μ	Modal frequencies in Hz					
			$L = 600$ mm			$L = 200$ mm		
			1	2	3	1	2	3
0.5	NTM	0.1	217.034	635.604	1267.590	1878.302	5163.860	9645.650
		0.4	232.036	797.543	1834.110	1995.497	6510.740	13831.40
		0.7	447.629	1037.270	2253.940	3813.426	8160	15739.200
	FE(3D)	0.1	216.987	634.850	1263.259	1876.267	5123.790	9448.138
		0.4	229.554	785.722	1819.305	1930.166	6271.645	13642.314
		0.7	437.591	1033.915	2245.125	3583.014	8091.330	15706.439
	% dev.	0.1	−0.022	−0.119	−0.343	−0.108	−0.782	−2.090
		0.4	−1.082	−1.504	−0.814	−3.385	−3.812	−1.386
		0.7	−2.294	−0.324	−0.392	−6.431	−0.849	−0.208
0.625	NTM	0.1	283.930	812.357	1608.220	2446.347	6532.940	11979.500
		0.4	308.616	991.955	2074.890	2639.638	7837.580	15025.700
		0.7	495.792	1128.820	2333.290	4167.385	8797.250	16074.300
	FE(3D)	0.1	283.898	811.795	1604.956	2445.458	6509.821	11855.709
		0.4	305.955	981.347	2072.554	2570.408	7647.979	15037.839
		0.7	489.234	1121.452	2336.177	4021.301	8655.042	16159.248
	% dev.	0.1	−0.011	−0.069	−0.203	−0.036	−0.355	−1.044
		0.4	−0.870	−1.081	−0.113	−2.693	−2.479	0.080
		0.7	−1.341	−0.657	0.123	−3.633	−1.643	0.526
0.750	NTM	0.1	355.027	993.279	1944.090	3030.222	7818.400	14004
		0.4	381.639	1149.720	2248.110	3236.367	8841.600	15842.900
		0.7	511.227	1230.890	2406.190	4268.272	9431.640	16437.800
	FE(3D)	0.1	355.036	993.179	1943.016	3031.657	7819.722	13978.716
		0.4	379.583	1144.159	2251.351	3181.291	8759.634	15934.664
		0.7	508.439	1224.396	2410.039	4205.930	9312.425	16529.197
	% dev.	0.1	0.002	−0.010	−0.055	0.047	0.017	−0.181
		0.4	−0.542	−0.486	0.144	−1.731	−0.936	0.576
		0.7	−0.548	−0.530	0.160	−1.482	−1.280	0.553
0.875	NTM	0.1	429.273	1177.820	2274.860	3616.212	9013.570	15741.600
		0.4	448.134	1269.840	2419.690	3759.295	9566.420	16569.700
		0.7	511.380	1312.660	2498.460	4253.660	9878.820	16849.800
	FE(3D)	0.1	429.347	1178.446	2277.013	3621.275	9047.347	15829.045
		0.4	447.258	1269.273	2423.695	3739.834	9595.934	16695.492
		0.7	510.778	1310.738	2502.153	4247.181	9870.045	16963.843
	% dev.	0.1	0.017	0.053	0.094	0.140	0.373	0.552
		0.4	−0.196	−0.045	0.165	−0.520	0.308	0.753
		0.7	−0.118	−0.146	0.148	−0.153	−0.089	0.672

between 0.5 and 0.7; that is, the step in the beam is located around the peak of the first free-free mode shape; see Figure 16(a). Figures 14(b) and 15(b) show that there are two peaks in Dev_2 prediction. The location of these peaks is found to be near the position of the peaks of the second free-free mode shape; see Figure 16(b). In addition, the value of Dev_2 approaches zero when the step location lies in the semistraight line between the two peaks in the second F-F mode shape. The same trend is repeated in the third mode shape as shown in Figures 14(c), 15(c), and 16(c). In addition, when the location of diametric step in shaft coincides with a peak point in i mode shape, the value of Dev_i is increased. Meanwhile, when the step lies in a straight portion of the mode shape, the Dev_i approaches zero.

3.4. Tapered Beam Approach. Due to the importance of tapered or conical beams in many engineering applications, the current section is devoted to show how to use the present analysis to solve the problem of taper beam. The current analysis is based on uniform beams, while the partial differential equation which represents the lateral vibration of tapered or conical beams is fourth-order Bessel equation [30,

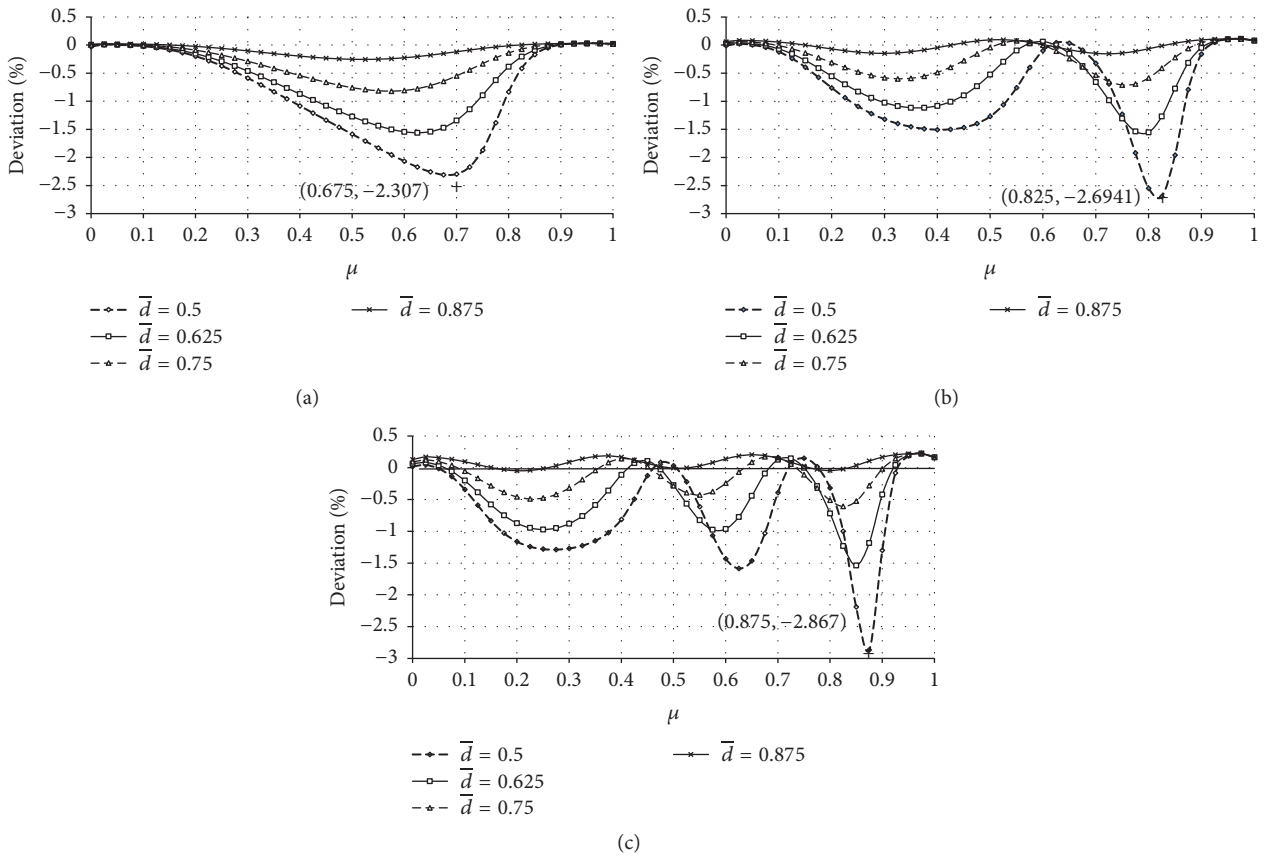

Figure 14: Variation of the percentage modal deviation between FE(3D) and NTM results as a function of μ and $\overline{d}$, for free-free long samples $L = 600$ mm: (a) 1st mode, (b) 2nd mode, and (c) 3rd mode.

31, 37, 38]. To simulate nonuniform beam using the current analysis, the beam is divided into multiple equal length spans as shown in Figure 17. The height and/or width of these spans are varying linearly between the start and the end to simulate the tapered or conical beam. The height and/or width ratio of i span can be calculated from the following formula:

$$h_{i1} = h_{n1} + (1 - h_{n1})\left(-\frac{x_i}{L} + \frac{L_{i1}}{2n}\right),$$
$$b_{i1} = b_{n1} + (1 - b_{n1})\left(-\frac{x_i}{L} + \frac{L_{i1}}{2n}\right), \quad (43)$$

where

$$h_{i1} = \frac{h_i}{h_1},$$
$$h_{n1} = \frac{h_n}{h_1},$$
$$b_{i1} = \frac{b_i}{b_1},$$
$$b_{n1} = \frac{b_n}{b_1},$$
$$L_{i1} = \frac{L_i}{L_1}. \quad (44)$$

h_i is the height of i beam segment and b_i is the width of i beam segment.

To verify the suitability of the current model to represent conical beams, the results of the current model are compared with the exact solution for cantilevered (C-F) conical beam with variable taper ratio $h_{n1} = b_{n1} = 0.2, 0.5$, and 0.7 as shown in Table 10. The model was investigated using the present NTM and using several number of spans $n = 20, 100, 200$, and 1000. The first three eigenvalues are evaluated for each taper ratio and number of spans. The time used for computing the first three natural frequencies is evaluated. The model results are also evaluated using NAT previously published in [6] at $n = 20$ in order to compare the time saving when using the present method.

The results of Table 10 show that increasing the number of spans results in increasing the accuracy of the evaluated beam eigenvalues in comparison with the exact solution in [30]. On the other hand, the results show that increasing the number of spans results in increasing the computational time. The comparison between the computational time using the present NTM and previously published NAT shows that the

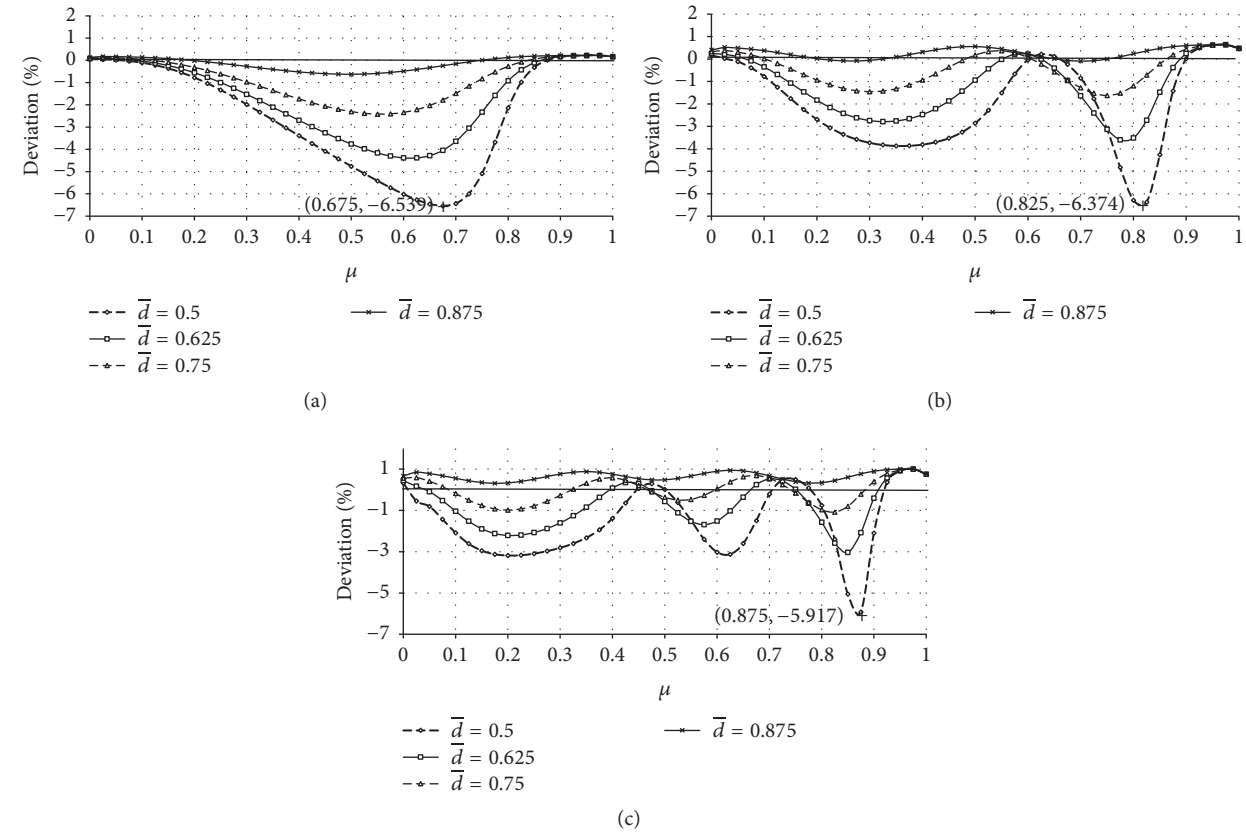

Figure 15: Percentage modal deviation between FE(3D) and NTM as a function of μ and $\overline{d}$, for free-free short samples $L = 200$ mm: (a) 1st mode, (b) 2nd mode, and (c) 3rd mode.

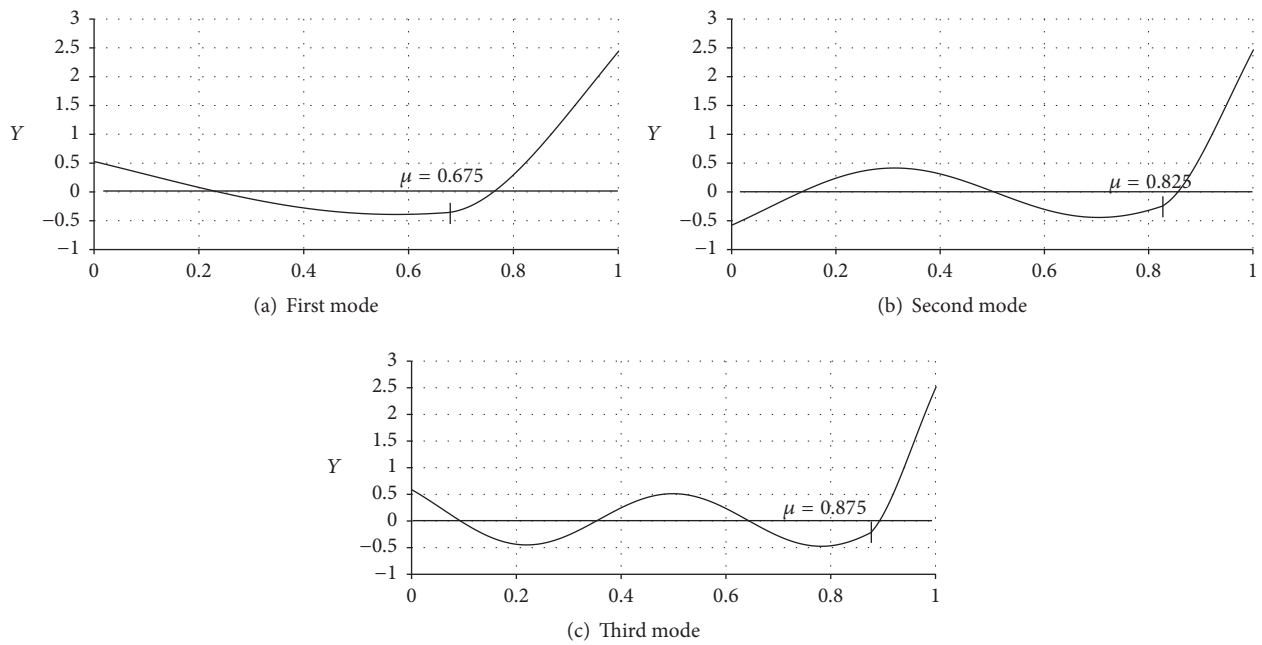

Figure 16: Typical first three modal shapes at the peak points shown in Figure 15 for free-free short sample and $\overline{d} = 0.5$.

Table 10: The first three eigenvalues for C-F conical beam using NTM in comparison with those of the exact solution presented in [30] and NAT results using the program of [6].

$h_{n1} = b_{n1}$		[30]	NAT [6] $n = 20$		NTM $n = 20$		NTM $n = 100$		NTM $n = 200$		NTM $n = 1000$	
				Time (s)		Time (s)		Time (s)		Time (s)		Time (s)
0.2	λ_1^{*2}	6.1964	6.1683	6	6.1706	1.8	6.1954	5.3	6.1962	10.5	6.1963	32.6
	λ_2^{*2}	18.3855	18.2513		18.2513		18.3801		18.3840		18.3853	
	λ_3^{*2}	39.8336	39.4809		39.4809		39.8194		39.8300		39.8336	
0.5	λ_1^{*2}	4.6252	4.6155	6.2	4.6175	1.9	4.6249	5.4	4.6250	10.9	4.6251	34
	λ_2^{*2}	19.5476	19.5074		19.5074		19.5460		19.5472		19.5477	
	λ_3^{*2}	48.5789	48.4725		48.4725		48.5746		48.5779		48.5788	
0.7	λ_1^{*2}	4.0669	4.0615	6.2	4.0635	1.9	4.0668	5.6	4.0669	11.1	4.0670	35
	λ_2^{*2}	20.5554	20.5360		20.5361		20.5547		20.5553		20.5554	
	λ_3^{*2}	—	53.9625		53.9625		54.0131		54.0147		54.0152	

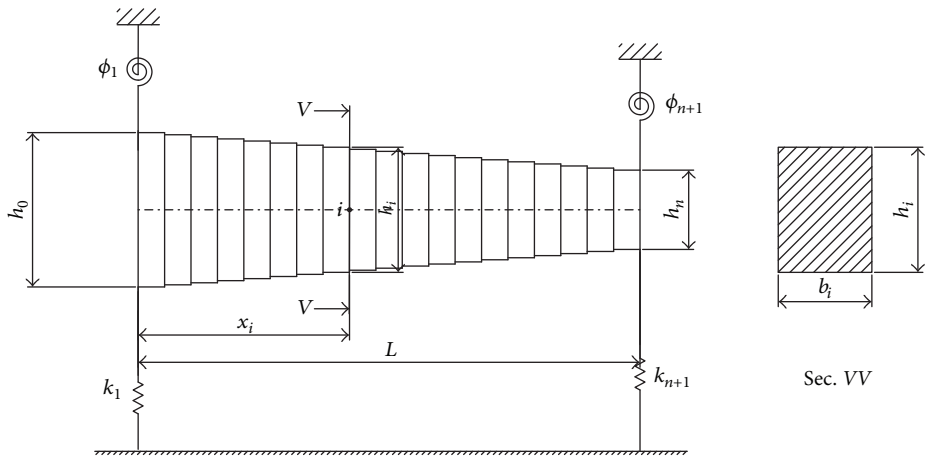

Figure 17: Stepped tapered beam with varying depth and width.

present NTM method is quicker than the NAT method [6] for the same number of spans.

To investigate the capability of the present model to evaluate the natural frequencies of taper or conical beam with variable boundary conditions, some cases of nonuniform beams are selected form [31]. The analysis in [31] is numerical and based on solving the taper beam partial differential equation using Runge-Kutta method. The boundary conditions and the taper ratio are listed in Table 11. The number of spans used in evaluating the current example is $n = 1000$. The eigenvalue results using the present NTM method are in good agreement with numerical results of [31].

Table 11: The first four eigenvalues for taper or conical beam subjected to variable end conditions using the present NTM and [31].

Beam parameters	Frequency parameter λ_1^{*2}	
	[31]	Present NTM
$h_{n1} = 1$ $Z_1 = Z_{n+1} = 10^8$ $\Phi_1 = 10^8, \Phi_{n+1} = 1000$	21.94	21.9518
	60.44	60.5461
	118.7	118.7589
	196.4	196.4162
$b_{n1} = 0.5$ $Z_1 = Z_{n+1} = 10$ $\Phi_1 = \Phi_{n+1} = 10^2$	4.98	5.0292
	12.50	12.4289
	40.13	39.8154
	88.28	88.0372
$b_{n1} = 1, h_{n1} = 1.5^{1/3}$ $Z_1 = 10^2, Z_{n+1} = 2 \times 10^2$ $\Phi_1 = 3 \times 10^2, \Phi_{n+1} = 4 \times 10^2$	13.63	13.6709
	24.59	24.9270
	48.37	48.7915
	97.28	97.5762
$b_{n1} = h_{n1} = 3^{1/4}$ $Z_1 = Z_{n+1} = 10^8$ $\Phi_1 = \Phi_{n+1} = 10^8$	25.83	25.8327
	71.00	71.1461
	139.3	139.4223
	230.3	230.4320

4. Conclusion

A new proposed normalized transfer matrix NTM uses new set of fundamental solution in combination with the transfer matrix method. This method has the advantage of the TMM in that the determinant of the frequency equation is 4×4 for n number of spans. In addition, the formation of the system frequency equation determinant is not included in any inverse matrix steps which reduces the computational time.

The current work introduces a comparison between the experimental and analytical NTM and three-dimensional finite element analyses for stepped thick beams. Different system parameters such as the step diameters ratio $\bar{d}$, the step location parameter μ, and the elastic segment length ratio L_2^* are considered. The following conclusions can be drawn from the present work:

(1) An excellent agreement between the present experimental results, using several test samples, and those of FE(3D) predictions has been recorded.

(2) The results show that the three-dimensional finite element can be trusted in the prediction of the modal frequencies of stepped thick beams in structural and mechanical system.

(3) An interesting percentage of modal deviations between the FE(3D) results and those obtained using the present frequency equation (40) has been illustrated. An increase in the step down location parameter (μ) and/or ($\bar{d}$) increases the modal deviations. The percentage deviations are higher for shorter beam than for longer one. The maximum deviation value in a specific normal mode is obtained when the step location is adjacent to a peak location in this normal mode. Moreover, the minimum percentage deviation in a specific mode shape is obtained when the step location lies in a straight portion in the mode shape. This may be explained by the smaller effect of stress concentration at the step under such conditions.

(4) Typical example shows that the computational time using normalized transfer matrix (NTM) is greatly reduced in comparison with numerical assembly technique (NAT).

In addition, to the above importance of conclusion, one can obtain accurate results for any combination of classical and elastic end conditions.

(5) Based on the stepped beam, the current analysis can be used to evaluate the results of tapered beam. The present NTM show a very good stability at very large number of spans which enables the accurate evaluation of the tapered beam results using stepped beam analysis.

Nomenclature

A: Cross-sectional area of the beam
a, b: Polynomial roots
d: Segment diameter
$\overline{d}$: Segment diameter ratio
E: Young's modulus of elasticity
f: Frequency (Hz)
G: Shear modulus of rigidity
I: Moment of inertia of the beam cross-section about the neutral axis
J_i: Rotational moment of inertia of the station mass
$\overline{J}_{i+1}$: $J_{i+1}/(\rho AL^3)_i$
$\acute{k}$: Shear deformation shape coefficient
k, ϕ: Elastic stiffness
k_1, k_{n+1}: End translational spring stiffness
L: Length of the beam (between points 1 and $n+1$)
L_i^*: Ratio L_i/L
m_i: Concentrated mass at i point
$\overline{m}_{i+1}$: $m_i/\rho_i A_i L_i$
m_t: Total mass of beam
r_1^{*2}: Rotary inertia parameter I_1/A_1L^2
s_1^{*2}: Shear deformation parameter $E_1 r_1^{*2}/G_1 k_1$
Y: Nondimensional lateral deflection
x, y: System coordinate of the beam
Z_1, Z_{n+1}: Nondimensional stiffness parameters defined as $k_1L_1^3/E_1I_1$ and $k_{n+1}L_n^3/E_nI_n$ respectively
Z_1^*, Z_{n+1}^*: Nondimensional stiffness parameters defined as k_1L^3/E_1I_1 and $k_{n+1}L^3/E_1I_1$ respectively
Γ_i: Nondimensional term $(Y_i' - L_i\Psi_i)$
δ_1, δ_2: Set of nondimensional terms defined as in (10a) and (10b)
λ_1^{*4}: Frequency parameter $(\rho_1 A_1 L^4 \omega^2/E_1I_1)$
λ_1^4: Frequency parameter $(\rho_1 A_1 L_1^4 \omega^2/E_1I_1)$
μ: Nondimensional beam length L_1/L
ν: Poisson's ratio
ξ: Nondimensional beam length x/L
ρ: Mass density of the beam material (kg/m^3)
ϕ_1, ϕ_{n+1}: End rotational spring stiffness
Φ_1, Φ_{n+1}: Nondimensional rotational spring parameters defined as $\phi_1 L_1/E_1I_1$ and $\phi_{n+1}L_n/E_nI_n$ respectively
Φ_1^*, Φ_{n+1}^*: Nondimensional rotational spring parameters defined as $\phi_1 L/E_1I_1$ and $\phi_{n+1}L/E_1I_1$ respectively
ψ: Slope due to bending
$(\cdot)'$: 1st derivative with respect to x or ξ
$(\cdot)''$: 2nd derivative with respect to$x$ or ξ
$(\cdot)'''$: 3rd derivative with respect to x or ξ
$(\cdot)''''$: 4th derivative with respect to x or ξ
C: Clamped (fixed) end
F: Free end
P: Pinned (hinged) end
S2: Two-span with single-step sample
S3: Three-span with two-step sample
vl: $10E+12$
vs: $10E-12$.

Conflicts of Interest

The authors declare that they have no conflicts of interest.

Acknowledgments

The authors gratefully thank the assistants, Eng. M. Zain, workshop technician, and office secretary for their technical support during all stages of this work.

References

[1] J. W. S. B. Rayleigh, *The Theory of Sound*, Macmillan, 1896.

[2] S. P. Timoshenko, "LXVI. On the correction for shear of the differential equation for transverse vibrations of prismatic bars," *The London, Edinburgh, and Dublin Philosophical Magazine and Journal of Science*, vol. 41, pp. 744–746, 1921.

[3] G. R. Cowper, "The Shear Coefficient in Timoshenko's Beam Theory," *Journal of Applied Mechanics*, vol. 33, no. 2, p. 335, 1966.

[4] S. K. Jang and C. W. Bert, "Free vibration of stepped beams: Higher mode frequencies and effects of steps on frequency," *Journal of Sound and Vibration*, vol. 132, no. 1, pp. 164–168, 1989.

[5] M. A. Koplow, A. Bhattacharyya, and B. P. Mann, "Closed form solutions for the dynamic response of Euler-Bernoulli beams with step changes in cross section," *Journal of Sound and Vibration*, vol. 295, no. 1-2, pp. 214–225, 2006.

[6] S. H. Farghaly and T. A. El-Sayed, "Exact free vibration of multi-step Timoshenko beam system with several attachments," *Mechanical Systems and Signal Processing*, vol. 72-73, pp. 525–546, 2016.

[7] H.-Y. Lin, "Dynamic analysis of a multi-span uniform beam carrying a number of various concentrated elements," *Journal of Sound and Vibration*, vol. 309, no. 1-2, pp. 262–275, 2008.

[8] Y. Yesilce, "Free and forced vibrations of an axially-loaded Timoshenko multi-span beam carrying a number of various concentrated elements," *Shock and Vibration*, vol. 19, no. 4, pp. 735–752, 2012.

[9] J. R. Banerjee, "Dynamic stiffness formulation for structural elements: a general approach," *Computers & Structures*, vol. 63, no. 1, pp. 101–103, 1997.

[10] S. Yuan, K. Ye, C. Xiao, F. W. Williams, and D. Kennedy, "Exact dynamic stiffness method for non-uniform Timoshenko beam vibrations and Bernoulli-Euler column buckling," *Journal of Sound and Vibration*, vol. 303, no. 3–5, pp. 526–537, 2007.

[11] E. B. Magrab, "Natural frequencies and mode shapes of Timoshenko beams with attachments," *Journal of Vibration and Control*, vol. 13, no. 7, pp. 905–934, 2007.

[12] J.-S. Wu and B.-H. Chang, "Free vibration of axial-loaded multi-step Timoshenko beam carrying arbitrary concentrated elements using continuous-mass transfer matrix method," *European Journal of Mechanics - A/Solids*, vol. 38, pp. 20–37, 2013.

[13] M. Attar, "A transfer matrix method for free vibration analysis and crack identification of stepped beams with multiple edge cracks and different boundary conditions," *International Journal of Mechanical Sciences*, vol. 57, no. 1, pp. 19–33, 2012.

[14] G. Ma, M. Xu, L. Chen, and Z. An, "Transverse free vibration of axially moving stepped beam with different length and tip mass," *Shock and Vibration*, vol. 2015, Article ID 507581, 2015.

[15] Q. S. Li, "Exact solutions for free longitudinal vibration of stepped non-uniform rods," *Applied Acoustics*, vol. 60, no. 1, pp. 13–28, 2000.

[16] Q. S. Li, J. Q. Fang, and A. P. Jeary, "Free vibration analysis of cantilevered tall structures under various axial loads," *Engineering Structures*, vol. 22, no. 5, pp. 525–534, 2000.

[17] Q.-P. Vu, J.-M. Wang, G.-Q. Xu, and S.-P. Yung, "Spectral analysis and system of fundamental solutions for Timoshenko beams," *Applied Mathematics Letters*, vol. 18, no. 2, pp. 127–134, 2005.

[18] R. H. Gutierrez, P. A. A. Laura, and R. E. Rossi, "Natural frequencies of a Timoshenko beam of non-uniform cross-section elastically restrained at one end and guided at the other," *Journal of Sound and Vibration*, vol. 141, no. 1, pp. 174–179, 1990.

[19] Y. Yesilce, "Differential transform method and numerical assembly technique for free vibration analysis of the axial-loaded Timoshenko multiple-step beam carrying a number of intermediate lumped masses and rotary inertias," *Structural Engineering and Mechanics*, vol. 53, no. 3, pp. 537–573, 2015.

[20] X. Wang and Y. Wang, "Free vibration analysis of multiple-stepped beams by the differential quadrature element method," *Applied Mathematics and Computation*, vol. 219, no. 11, pp. 5802–5810, 2013.

[21] F. Ju, H. P. Lee, and K. H. Lee, "On the free vibration of stepped beams," *International Journal of Solids and Structures*, vol. 31, no. 22, pp. 3125–3137, 1994.

[22] P. A. A. Laura and R. H. Gutierrez, "Analysis of vibrating Timoshenko beams using the method of differential quadrature," *Shock and Vibration*, vol. 1, no. 1, pp. 89–93, 1993.

[23] A. Shahba, R. Attarnejad, and S. Hajilar, "Free vibration and stability of axially functionally graded tapered Euler-Bernoulli beams," *Shock & Vibration*, vol. 18, no. 5, pp. 683–696, 2011.

[24] J. W. Jaworski and E. H. Dowell, "Free vibration of a cantilevered beam with multiple steps: Comparison of several theoretical methods with experiment," *Journal of Sound and Vibration*, vol. 312, no. 4-5, pp. 713–725, 2008.

[25] Q. Mao and S. Pietrzko, "Free vibration analysis of stepped beams by using Adomian decomposition method," *Applied Mathematics and Computation*, vol. 217, no. 7, pp. 3429–3441, 2010.

[26] Q. Mao, "Free vibration analysis of multiple-stepped beams by using Adomian decomposition method," *Mathematical and Computer Modelling*, vol. 54, no. 1-2, pp. 756–764, 2011.

[27] Z. R. Lu, M. Huang, J. K. Liu, W. H. Chen, and W. Y. Liao, "Vibration analysis of multiple-stepped beams with the composite element model," *Journal of Sound and Vibration*, vol. 322, no. 4-5, pp. 1070–1080, 2009.

[28] K. Suddoung, J. Charoensuk, and N. Wattanasakulpong, "Application of the differential transformation method to vibration analysis of stepped beams with elastically constrained ends," *Journal of Vibration and Control*, vol. 19, no. 16, pp. 2387–2400, 2013.

[29] G. Duan and X. Wang, "Free vibration analysis of multiple-stepped beams by the discrete singular convolution," *Applied Mathematics and Computation*, vol. 219, no. 24, pp. 11096–11109, 2013.

[30] S. Naguleswaran, "A Direct Solution for the Transverse Vibration of Euler-Bernoulli Wedge and Cone Beams," *Journal of Sound and Vibration*, vol. 172, no. 3, pp. 289–304, 1994.

[31] B. K. Lee, J. K. Lee, T. E. Lee, and S. G. Kim, "Free vibrations of tapered beams with general boundary condition," *KSCE Journal of Civil Engineering*, vol. 6, no. 3, pp. 283–288, 2002.

[32] R. E. Rossi, P. A. A. Laura, and R. H. Gutierrez, "A note on transverse vibrations of a Timoshenko beam of non-uniform thickness clamped at one end and carrying a concentrated mass at the other," *Journal of Sound and Vibration*, vol. 143, no. 3, pp. 491–502, 1990.

[33] S. H. Farghaly, "Vibration and stability analysis of Timoshenko beams with discontinuities in cross-section," *Journal of Sound and Vibration*, vol. 174, no. 5, pp. 591–605, 1994.

[34] S. H. Farghaly and T. A. El-Sayed, "Exact free vibration analysis for mechanical system composed of Timoshenko beams with intermediate eccentric rigid body on elastic supports: An experimental and analytical investigation," *Mechanical Systems and Signal Processing*, vol. 82, pp. 376–393, 2017.

[35] A. Díaz-De-Anda, J. Flores, L. Gutiérrez, R. A. Méndez-Sánchez, G. Monsivais, and A. Morales, "Experimental study of the Timoshenko beam theory predictions," *Journal of Sound and Vibration*, vol. 331, no. 26, pp. 5732–5744, 2012.

[36] J. n. Vaz and J. de Lima, "Vibration analysis of Euler-Bernoulli beams in multiple steps and different shapes of cross section," *Journal of Vibration and Control*, vol. 22, no. 1, pp. 193–204, 2016.

[37] H. H. Mabie and C. B. Rogers, "Transverse Vibrations of Tapered Cantilever Beams with End Support," *The Journal of the Acoustical Society of America*, vol. 44, no. 6, pp. 1739–1741, 1968.

[38] S. M. Ibrahim, S. H. Alsayed, H. Abbas, E. Carrera, Y. A. Al-Salloum, and T. H. Almusallam, "Free vibration of tapered beams and plates based on unified beam theory," *Journal of Vibration and Control*, vol. 20, no. 16, pp. 2450–2463, 2014.